Ph.D. dissertation

# Foam Glass for Construction Materials: Foaming Mechanism and Thermal Conductivity

by

Rasmus Rosenlund Petersen

Department of Chemistry
and Bioscience
Aalborg University, Denmark

AALBORG UNIVERSITY
DENMARK

Dissertation submitted

Date of Defence:
July 31st, 2015

Assessment committee

**Alicia Durán**
Professor
Istituto de Cerámica y Vidrio
(CSIC), Spain

**Cristina Leonelli**
Professor
University of Modena and Reggio
Emilia, Italy

**Vittorio Boffa**
Associate Professor
Aalborg University

PhD supervisor

**Yuanzheng Yue**
Professor
Aalborg University

| | |
|---|---|
| Thesis submitted: | June 15, 2015 |
| PhD supervisor: | Prof. Yuanzheng Yue<br>Aalborg University, Denmark |
| PhD committee: | Prof. Alicia Durán<br>Instituto de Cerámica y Vidrio (CSIC), Spain |
| | Prof. Cristina Leonelli<br>University of Modena and Reggio Emilia, Italy |
| | Associate Prof. Vittorio Boffa<br>Aalborg University, Denmark |
| PhD Series: | Faculty of Engineering and Science<br>Aalborg University |

ISSN: xxxx- xxxx
ISBN: xxx-xx-xxxx-xxx-x

Published by:
Aalborg University Press
Skjernvej 4A, 2nd floor
DK – 9220 Aalborg Ø
Phone: +45 99407140
aauf@forlag.aau.dk
forlag.aau.dk



Printed in Denmark by Rosendahls, 2014

# Preface and Acknowledgements

This thesis has been submitted for assessment in partial fulfillment of the PhD degree. The thesis is based on submitted published scientific papers which are listed in section 1. Parts of the papers are used directly or indirectly in the extended summary of the thesis. As part of the assessment, co-author statements have been made available to the assessment committee and are also available at the Faculty. The thesis is not in its present form acceptable for open publication but only in limited and closed circulation as copyright may not be ensured.

The study is part of an interdisciplinary CleanTechBlock project financed by the The Advanced Technology Foundation (Højteknologifonden). The CleanTechBlock is an interdisciplinary collaboration between Section of Chemistry (Aalborg University), Murværk (Danish Technological Institute), Gråsten Brickwork A/S and Egernsund Tegl.

I would like to thank my supervisor Yuanzheng for his guidance and inspiration throughout the PhD project. I really enjoyed our collaboration. I wish to thank Jakob König from Jozef Stefan Institute (Slovenia), a former Post Doc at the glass group and participant in the CleanTechBlock project. We have had countless of discussions about instruments and equipment design, preparation procedures and process parameters.

My kind acknowledgements go to the people at Danish Technological Institute (DTI), Gråsten Brickwork (GB) and Egernsund Tegl for a very pleasant cooperation. Special credit goes to Helge Hansen (DTI) for valuable discussions and XRF measurements, Christian Prinds (DTI) for preparing and measuring thermal conductivity of foam glasses and Jacob Bendtsen (GB) for providing glass powder. I would also like to thank Hansjörg Börnhöft (Technische Universität Clausthal) for help with the Heating Microscope and Kim Lykke (Reiling Glasrecycling) for introducing me to their glass recycling facility.

I wish to thank my fellow PhD students: Christian Hermansen, Jonas Kjeldsen, Thuy Thanh Do, Ali Farsi, Rene Mossing Thomsen, Kim Thomsen, Laura Paraschiv, Mouritz Nolsøe Svenson, Hao Liu. Thank you for creating an enjoyable atmosphere.

Finally, a special thank goes to my wife Aurora S. Prawiradinata for being very patient and enduring our long distance relationship in first period of the Ph.D. period.

# English Abstract

Foam glass has been used for over 70 years in construction and industry for thermal insulation. Foam glass is mainly made of recycle glass. Strict energy policy motivates foam glass manufactures to improve the thermal insulation of foam glass. The effort to understand the making of foam glass with good insulation ability is scarcely reported. The goal of this Ph.D. thesis is to reveal the underlying mechanism of foaming reaction, foam growth and the heat transport of solid foam glass. In this thesis, the panel glass from cathode ray tubes (CRT) will serve as a key material to reveal the mechanisms.

Foaming is commonly achieved by adding metal oxides or metal carbonates (foaming agents) to glass powder. At elevated temperature, the glass melt becomes viscous and the foaming agents decompose or react to form gas, resulting in foamy glass melt. Subsequent cooling to room temperature, lead to solid foam glass. Metal carbonates decompose due to surface reaction. Based on $Na_2CO_3$, we show the reaction is fast and the glass transition is changed considerably. We propose the reaction rate is dependent on contact area between glass melt and $Na_2CO_3$, melt viscosity and $Na^+$ diffusion.

A method is developed for optimising process parameters. Characteristic temperatures are derived from a deformation curve and the deformation rate curve. Maximum expansion rate was linked to closed porosity. Using this knowledge the method is applied to literature data to analyse for optimal conditions. The resulting conditions were in agreement with industrial conditions. Since no foam glass properties are necessary to measure, the method allows fast investigation of process parameters.

The melt viscosity is an important parameter for foam growth. We compared bubble- and crystal free melt viscosity with foam density and show in order to minimise the foam density, the heat-treatment should be performed in the viscosity regime of $10^{3.7}$-$10^6$ Pa s.

The thermal conductivity of foam glass made is often reported to be linear dependent on porosity or foam density. Foam glasses made from CRT panel glass and different foaming agents confirm this trend at high porosity level (85-97%). The experimental data suggests the solid conductivity is dependent on the foaming agent applied.

# Resumé (Danish Abstract)

Skumglas har været brugt som termisk isolerende materiale i over 70 år i konstruktions- og industrimæssige sammenhæng. Skumglas består hovedsageligt af genbrugsglas. Streng energipolitik har motiveret skumglasproducenter til at forbedre isoleringsevnen på skumglas. Der er få rapporteret forsøg på at forstå og forbedre isoleringsevnen. Målet med denne Ph.D. afhandling er at vise mekanismerne, som styrer gas udvikling, skumdannelse og varmetransporten i faste skumglas. I denne afhandling, vil panelglasset fra billedrør spille en central rolle til at forstå mekanismerne.

Opskumning opnås sædvanligvis ved at tilføre metaloxider eller karbonat-salte (skumningsagenter) til glas pulver. Ved høje temperature bliver glasset flydende og skumningsagenterne dekomponerer eller reagerer, som derved udløser gas. Dette resulterer i opskumning af glassmelten. Efterfølgende afkøling til rumtemperatur, resulter i et fast skumglas. Karbonatsalte dekomponerer som et resultat af overfladereaktion på glassmelten. Baseret på $Na_2CO_3$, viser vi at reaktion er hurtig og at glasovergangstemperaturen ændres mærkbart. Vi foreslår at reaktionen er afhængig af overfladekontakt mellem smelten og $Na_2CO_3$, smelteviskositeten og $Na^+$ diffusion.

En metode er udviklet til at optimere procesparametrene. Karakteristiske temperature er afledt fra deformeringskurver og hastighedskurver. Maximal opskumningshastighed var sammenkædet med den lukkede porøsitet. Denne metode kunne analysere litteratur data og de optimale proces parametre kunne bestemmes. Resultatet var i overensstemmelse med industrielle data. Siden ingen skumglasegenskaber skal måles for at bruge metoden, så kan metoden potentielt forøge forskningshastigheden.

Smelteviskositeten er en vigtig parameter for opskumning. Sammenligning af boble- og krystal fri smelteviskositet med skumdensiteten viste at varme-behandlingen bør foretages i viskositetsområdet $10^{3.7}$-$10^6$ Pa s for at minimere skumdensiteten.

Den termiske ledningsevne er ofte rapporteret som værende lineær afhængig af densiteten. Skumglas lavet af panelglas og forskellige skumningsagenter bekræftede denne trend til dels i et bredt porøsitetsspænd (85-97%). De eksperimentelle data antyder at ledningsevnen af den faste del er afhængig alt efter hvilken skumningsagent som bliver brugt.

# Table of Contents

# 1. Introduction

Mankind has always had a need for insulation, making clothing to keep warm and building homes to survive through harsh winters. In modern civilisation, glass is an important insulation material for house construction. Insulation material made of glass combines good insulation ability with excellent thermal stability. Man-made glass fibres or mineral wool have been available since the 18$^{th}$ century as insulation material and are today one of the preferred materials. Porous glass (or foam glass) dates to the 1930's [1]. In comparison to the glass fibres, foam glass had a more anonymous role as insulation material through the history.

Foam glass is a kind of inorganic material formed by freezing a bubble-containing glass melt. Glass powder is commonly employed as precursor and when mixed together with a solid or fluid foaming agent, bubbles form in the glass melt at elevated temperatures. The porous structure of foam glass makes it ideal for thermal applications owing to much lower thermal conductivity of the gas in the bubbles compared to the glass itself.

In the last two decades foam glass material has gained an increased attention. This is because the environment plays an ever more important role and the foam glass process has become a valuable solution for reprocessing waste glass. Landfilling the waste glass has long been a common practice, but cost of landfilling has increased. At the same time energy prices have increased, and therefore waste glass has become a vital resource for glass manufactures and an important sales product for glass recyclers. The glass recyclers sort and clean the waste glass. The cleaning process leaves fractions of glass which are too costly to clean. These "dirty" fractions have no value for the float and bottle glass industry and it is therefore commonly landfilled. The foam glass industry, however, is able to use waste glass containing up to 5 wt% of impurities, such as ceramic, stone, colorants and porcelain, if the waste materials are finely grinded.

Container glass and flat glass have already an established closed recycle loops, i.e. most of the post-consumer glass returns to the manufactures [2]. However, Cathode ray tube (CRT) glasses from outdated televisions and computers monitors have almost no recycling loops [3-5]. Instead, waste glass from CRTs accumulates on landfills [6] and become an increasing environmental problem [4]. CRT glass consists of multiple glass compositions (**Fig. 1.1**): 65 wt% panel glass, 30 wt% funnel glass, 5 wt% neck glass and < 1 wt% frit glass [4]. The panel glass is connected to the

funnel with a glass frit [4]. The neck-, funnel-, and frit glass contains a high amount of lead. Panel glass can contain lead if the screens originate from black and white televisions [3,7]. In colour television, most panel glasses do not contain lead, since majority of CRT manufactures converted into non-lead panel glass production after 1995 [3]. Lead is banned in many applications and will be restricted in construction materials within EU [8]. Hence, neck-, funnel-, and frit glasses can only be used if lead is extracted through alkaline leaching [9], carbothermal treatment [10] or through the energy intensive smelting process [5,11,12]. The panel glass from colour television can, however, potentially be reutilised in the foam glass production. Glass recyclers can easily separate non-lead glass from lead glass through optical sorting systems [5,6]. Panel glass produced after 1993 contains BaO and SrO and they are not restricted in building materials in Denmark. Leaching test of CRT panel glass powder and crushed foam glass show that the BaO and SrO remains stable incorporated in the glass [13].

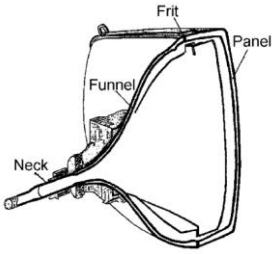


**Fig. 1.1 –** Cathode ray tube (CRT) consist of four different glasses: Neck, Funnel, frit and panel. Picture is from [14].

The overall aim of this Ph.D. project is to develop foam glasses as thermal insulating material for house walls. The project is part of larger interdisciplinary collaboration between Danish Technological Institute, Gråsten Brickwork and Egernsund Tegl. The overall aim of the project is to develop a new wall technology, i.e., to make a new type of integrated building block, CleanTechBlock, which consists of foam glass sandwiched between two clay bricks (**Fig. 1.2**). Denmark is restricting the household energy consumption to one of the lowest levels in the world, encouraging architects to use high-performing thermal insulation or to increase the amount of insulation. High-performing insulation materials are very expensive and are very often not cost-effective. Instead, contractors are forced to improve the insulation by increasing the amount of conventional insulation material. The building block is intended to meet the forthcoming market standards by providing a slim wall solution and fast construction speed. The foam glass is suitable as insulation material, since it cannot burn,

is impermeable to wind and water, resistant against freeze-thaw and durable against vermin.

a)  b) 

**Fig. 1.2** – a) Mock-up of a wall section consisting of b) foam glass sandwiched between two red clay bricks.

## 1.1 Background and Challenges

The foaming of glass melt is a complicated matter. Many parameters control the foaming process: Temperature, time, gas atmosphere, gas pressure, viscosity, surface tension and crystallisation ability of glass composition, particle size, concentration and type of foaming agent. Hence, optimising the foaming process is very difficult and time consuming.

Foams are also very complex systems to study. They are formed and exist under non-equilibrium conditions and the foams will tend to minimise surface energy through coalescence and eventually collapsing. Hence, their lifetime is limited. Most foam systems consist of stable liquids (e.g. water, oil). Glass melts are foamed in the viscosity range of $10^{3.6}$-$10^{6}$ Pa s. In this range, the glass melt is meta-stable and can tend to crystallise. This makes the understanding of foaming ability of glass melts more complicated.

The vast majority of foam glass research focuses on demonstrating which natural resources or waste materials can act as melt precursors (e.g. ash, blast furnace slags, red mud, waste glass) or foaming agent (e.g. egg shells, saw dust, oil waste, plaster boards, metal carbonates and -oxides). The growing industrial activities are followed by an increasing interest from academic researchers. This is exemplified in the growing publication rate from year 2000 (**Fig. 1.3**). In addition, new and established companies have constructed many new factories in Europe in the last two decades to meet the growing demand.

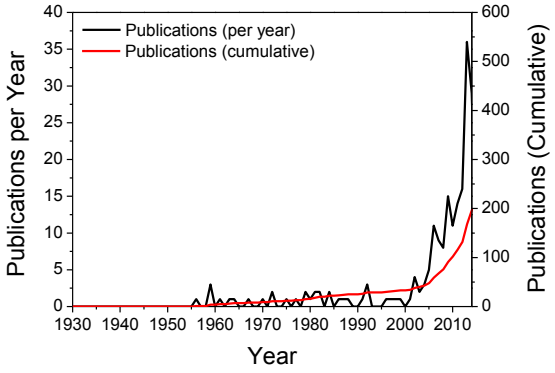


**Fig. 1.3** - Number of publications in English peer-review journals which report on the preparation, characterisation and modelling of foam glass.

The goal of this PhD project is to gain understanding of the reaction mechanism, foam dynamics and thermal conductivity. The aim is to open up for new strategies to improve insulation ability of foam glass. The thermal conductivity can be lowered by decreasing density, optimising pore structure, altering the composition of the entrapped gas and improving the glass matrix. There are several publications reporting on the thermal conductivity of foam glass, but very few researches discuss the possible parameters influencing the thermal conductivity of foam glasses [15-17] and how to improve the thermal insulation. It is only sensible to discuss the thermal conductivity if the foam glasses are well characterised, i.e. if the pore structure, gas composition and solid matrix are well defined. This Ph.D. project focuses on three topics:

1) The insulation ability can be improved by incorporating low conducting gasses in the foam. The choices of foaming agents directly influence the resulting gas composition. However, gas entrapment is only sensible if the pores remain closed. Foams are thermodynamically unstable due to their high surface area (and surface energy). Hence, the pores minimise the surface area through a coalescence process, which transforms the pores from being closed to open. Thus, the foam glass will eventually become percolated. My task is to define criteria for making foam glasses with closed pores. The task focuses on reaction mechanism and foam dynamics.

2) A wide range of waste materials and natural resources have potential to form the foam glass production. It is time consuming to optimise a recipe, since many parameters control the foaming process. The

temperature influence on both bubble growth and coalescence and is one of the most important factors to consider. Therefore, another task of this project is to define the foaming ability in terms of temperature and viscosity regime in which foaming should proceed.

3) The thermal conductivity of foam glass is an important property for thermal insulation applications, but few systematic results are reported. Hence, the mechanism controlling the heat transport remains almost an untouched issue. A third task is to reveal the impact of solid and gaseous conductance on the overall thermal conductivity.

## 1.2 Objectives

The overall goal of this PhD project is to understand the reaction mechanism, viscosity and foam dynamics controlling the structural properties and the thermal conductivity of foam glass.

The CRT panel glass is a key waste material in the CleanTechBlock project. Therefore, the feasibility of using CRT panel glass in a foam glass production is discussed. In relation to this, the chemical composition, viscosity and glass stability of CRT panel glass are discussed in relation to foaming ability and thermal conductivity.

The reaction mechanism and foam dynamics are studied on CRT panel glass foamed with $Na_2CO_3$ and $MnO_2$. A reaction mechanism is proposed for metal carbonates and metal oxides.

The role of glass melt viscosity is studied to link this property to the foaming ability. Labware, E-glass, CRT panel glass and soda-lime-silica glass are foamed with $CaCO_3$ at isokom temperatures to reveal the viscosity regime of foaming.

The thermal conductivity of foam glass is studied to reveal the impact of foaming agent on the overall thermal conductivity. The foam glass a made from CRT panel glass and $MnO_2$ and $CaCO_3$ as foaming agent. This is done with aim to idealise the gas and the solid composition.

The objectives of the Ph.D. thesis are summarised below:

1) Reveal the feasibility of using CRT panel glass in a foam glass production.

2) Suggest reaction mechanism for metal carbonates and transition metal oxides and reveal the relationship between reaction mechanism and foam structure.

3) Relate the foaming ability to bubble- and crystal free glass melt viscosity and clarify any universal viscosity regime for foaming of glass melt.

4) Reveal the impact of foaming agent on thermal conductivity of foam glass and account for how gas- and glass composition influence the thermal conductivity of foam glass.

### 1.3 Thesis Content

The thesis consists of an overview thesis and three published peer-reviewed papers (see the list below). These papers are cited throughout out the thesis using roman numerals.

I. R.R.Petersen, J. König, Y.Z. Yue, The Mechanism of Foaming and Thermal Conductivity of Glasses Foamed with $MnO_2$, J. Non-Cryst. Solids 425 (2015) 74.

II. R.R.Petersen, J. König, M.M. Smedskjaer, Y.Z. Yue, Effect of $Na_2CO_3$ as Foaming Agent on Dynamics and Structure of Foam Glass Melts, J. Non-Cryst. Solids, 400 (2014) 1.

III. R.R.Petersen, J. König, M.M. Smedskjaer, Y.Z. Yue, Foaming of CRT panel glass powder using $Na_2CO_3$, Glass Tech.: Eur. J. Glass Sci. Tech. Part A, 55 (2014) 1.

# 2. Foaming of Glass Melts

Low density foam glass with closed pores is a challenge to obtain. Some foaming agents have shown to more suitable for forming low density foam glass. Transition metals, such as $MnO_2$ [18-21] and $Fe_2O_3$ [21-23] are easy to form low density foam glass of float glass and CRT panel glass, whereas carbonates, such as $Na_2CO_3$ (**Fig. 2.1)** and $CaCO_3$, are difficult to make foam glass melts with density lower than 0.2 g/cm$^3$. $Na_2CO_3$ and $CaCO_3$ are readily available resources and the formation of $CO_2$ enables good thermal insulation. Despite $CaCO_3$ being one of the most reported foaming agent within the scientific literature and in patents, low density foam glass cannot be achieved with $CaCO_3$.

## 2.1 Glass resources

In order to introduce CRT panel glass in industrial production, the viscosity and glass stability (resistance to crystallisation) should remain stable between the CRT televisions. Therefore, the chemical composition cannot fluctuate. The CRT waste stream quality collected at the electronic recycler Averhoff A/S (Århus, Denmark) show a very stable chemical composition (**Table 2.1**).

**Table 2.1 –** Chemical compositions of several Cathode Ray Tube (CRT) panel glasses. The CRT panel glass from the same producer can originate from different factories.

| # | Producer | Chemical composition [wt%] | | | | | | | | | | |
|---|---|---|---|---|---|---|---|---|---|---|---|---|
| | | $SiO_2$ | $Al_2O_3$ | $Fe_2O_3$ | $Na_2O$ | $K_2O$ | CaO | MgO | SrO | BaO | $ZrO_2$ | SUM |
| 1 | LG Phillips Displays | 60.1 | 2.99 | 0.07 | 8.4 | 6.54 | 0.69 | 0.41 | 8.57 | 8.93 | 2.38 | 99.1 |
| 2 | Philips Displays | 60.0 | 2.63 | 0.05 | 8.0 | 6.55 | 0.69 | 0.33 | 8.47 | 8.69 | 2.38 | 97.8 |
| 3 | Phillips Displays | 60.5 | 2.80 | 0.13 | 8.1 | 6.62 | 0.64 | 0.32 | 8.49 | 8.74 | 2.38 | 98.7 |
| 4 | Thompson | 61.2 | 2.12 | 0.06 | 7.6 | 6.73 | 0.28 | 0.01 | 8.84 | 9.88 | 1.46 | 98.2 |
| 5 | Thompson | 60.6 | 2.16 | 0.07 | 7.7 | 6.83 | 0.19 | 0.01 | 8.91 | 9.96 | 1.45 | 97.8 |
| 6 | Sony Triniton | 60.8 | 2.12 | 0.13 | 7.02 | 7.58 | 0.17 | 0.05 | 9.46 | 8.84 | 1.43 | 97.6 |
| 7 | Phillips | 60.3 | 2.12 | 0.10 | 7.34 | 7.21 | 0.18 | 0.03 | 9.15 | 9.36 | 1.43 | 97.2 |
| 8 | Panasonic | 59.8 | 3.01 | 0.09 | 7.54 | 7.18 | 0.12 | 0.01 | 8.72 | 10.01 | 1.33 | 97.8 |
| 9 | Hitachi | 60.6 | 2.06 | 0.05 | 7.38 | 7.23 | 1.08 | 0.28 | 8.21 | 9.09 | 2.36 | 98.3 |
| 10 | Sanyo | 59.6 | 1.91 | 0.04 | 7.67 | 6.95 | 1.80 | 0.42 | 8.06 | 9.31 | 2.47 | 98.3 |
| 11 | Orion | 61.6 | 2.02 | 0.07 | 7.02 | 7.55 | 0.06 | 0.00 | 9.25 | 8.93 | 1.56 | 98.0 |
| 12 | Samsung | 60.2 | 2.22 | 0.08 | 7.08 | 7.59 | 0.10 | 0.04 | 9.21 | 8.93 | 1.59 | 97.0 |
| 13 | Sony Triniton | 61.5 | 1.91 | 0.06 | 7.17 | 7.65 | 0.06 | 0.00 | 9.45 | 9.18 | 1.44 | 98.3 |
| 14 | Samsung | 61.0 | 2.08 | 0.04 | 7.43 | 7.04 | 0.07 | 0.00 | 9.04 | 9.99 | 1.37 | 98.1 |
| | Average | 60.5 | 2.3 | 0.1 | 7.5 | 7.1 | 0.4 | 0.1 | 8.8 | 9.3 | 1.8 | 98.0 |
| | Min | 59.6 | 1.9 | 0.0 | 7.0 | 6.5 | 0.1 | 0.0 | 8.1 | 8.7 | 1.3 | 97.0 |
| | Max | 61.6 | 3.0 | 0.1 | 8.4 | 7.6 | 1.8 | 0.4 | 9.5 | 10.0 | 2.5 | 99.1 |

## 2.2 General Preparation procedure

Glass is crushed with jaw crusher and ball milling or crushed at external partners using rolling mills. Particle size of glass and foaming agent is important for the foaming ability [16], foam density [18,24-27] and closed porosity [24]. Mixing is performed either with ball mill or together with balls in a plastic container spinned on a roundabout. Unlike industrial production, the powder was compacted by pressing the powder in a steel mould with 40 MPa (**Fig. 2.1**). The pressure is much larger than what is applied industrially, if any pressure is applied at all. However, compressing the powder prior to heat-treatment improves reproducibility.

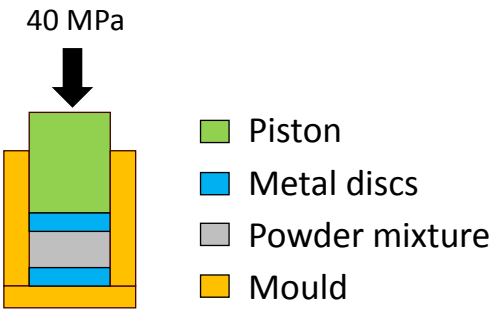


**Fig. 2.1 –** Uniaxial compaction of powder mixture in a steel mould. The pellet diameter was either 13 mm or 30 mm.

The foaming takes place on stainless steel coated with kaolin to prevent sticking of glass melt to the steel. Small (1 g) and large (40 g) foam glasses are prepared by heating without a mould (small samples) and by foaming in moulds (large samples). Foam glasses for thermal conductivity measurements required large size samples (Ø = 60 mm). Therefore, they were formed in moulds of 6 cm diameter.

The foam density ($\rho_{foam}$) was either determined from the diameter, height and mass of the foam cylinders or by using Archimedes method in water or ethanol. The powder density of the crushed foam glass ($\rho_{pow}$) was measured with a He-Pycnometer (Ultrapyc 1200e, Quantachrome). $\rho_{pow}$ and $\rho_{foam}$ were used to calculate the porosity, $\varphi$:

$$\varphi = \left(1 - \frac{\rho_{foam}}{\rho_{pow}}\right) \cdot 100\% \qquad (2.1)$$

The skeletal density ($\rho_{skel}$) was measured on core drilled foam cylinders (height = 30–32 mm, Ø = 38 mm) with a He-pycnometer. The skeletal density was used to calculate closed porosity, $\varphi_{cp}$:

$$\varphi_{cp} = \frac{{\rho_{skel}}^{-1} - {\rho_{pow}}^{-1}}{{\rho_{foam}}^{-1} - {\rho_{pow}}^{-1}} \cdot 100\% \qquad (2.2)$$

## 2.3 Foaming with $Na_2CO_3$

$Na_2CO_3$ starts to decompose when it melts at 1098 K. The decomposition remains slow up to 1273 K [28]. When mixed with CRT panel glass, foaming occurs at 973 K, well below the thermal decomposition temperature. Hence, the decomposition can be ascribed to a surface reaction between the glass melt and $Na_2CO_3$. The foam density exhibits a minimum when foamed at different temperatures (**Fig. 2.2)**.

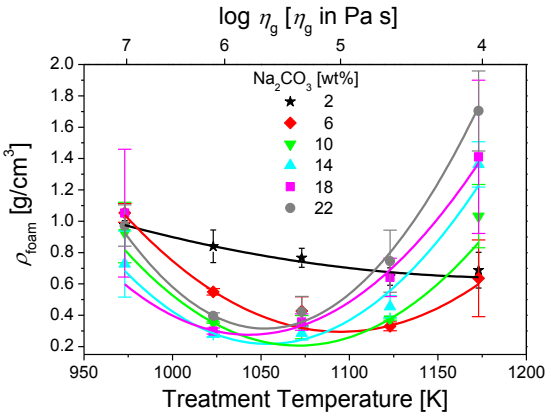


**Fig. 2.2** – Foam density ($\rho_{foam}$) of foam glass prepared with different $Na_2CO_3$ concentration at different treatment temperature (see legend). The logarithmic viscosity (log $\eta_g$) corresponds to the untreated glass melt viscosity of CRT panel glass (#1 in **Table 2.1**). [Paper III]

Not all the foam glasses remained amorphous. When relative high concentration of $Na_2CO_3$ is used (14-22wt%), the foam glasses partial crystallise $Na_2SrSi_2O_5$ (**Fig. 2.3a**). The $Na_2CO_3$ could provide nucleation sites for crystallisation. The crystallisation degree increases with the $Na_2CO_3$ amount. This effect could however be caused because the solubility limit of $Na_2O$ is reached and crystallisation degree is maximised. This could also explain why the crystallisation degree is apparently not changing when temperature is varied between 973 – 1173 K (**Fig. 2.3b**) and when treatment time is varied (**Fig. 2.4**). It should be noted that $Na_2O$ cannot be detected with XRD since it is amorphous [29].

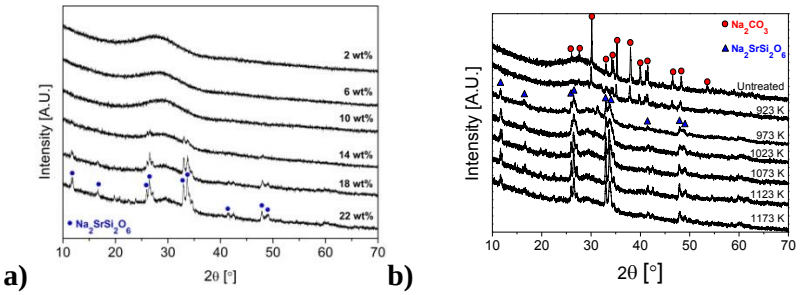


**Fig. 2.3** – XRD patterns of foam glasses prepared by heat-treatment for 45 min **a)** at 1073 K for different concentrations (see legend) [Paper III] and **b)** with 22 wt% $Na_2CO_3$ at different temperatures (see legend) [Paper II]. The XRD spectra are shifted vertically for clarity.

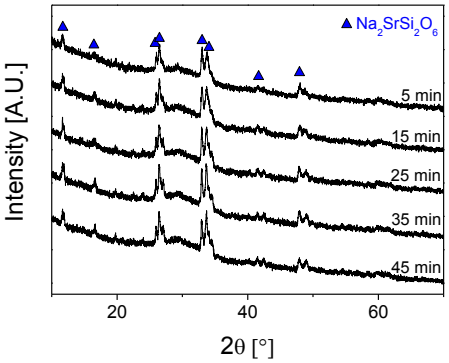


**Fig. 2.4** - XRD patterns of foam glasses prepared with 22 wt% $Na_2CO_3$ by heat-treatment at 1073 K for different durations (see legend). Blue triangles identify $Na_2SrSi_2O_6$ crystals. The XRD spectra are shifted vertically for clarity. [Paper II]

The foam glasses collapses at high temperatures (> ~1100 K) but this is only observed when $Na_2CO_3$ concentration reaches ≥6wt%. The degree of collapse (increasing density) increases with increasing amount of $Na_2CO_3$. $Na_2O$ is known to provide non-bridging oxygen to the glass structure by depolymerising the [$SiO_4$] network which leads to a decrease of viscosity. The depolymerisation effect is clearly reflected in a drop in the glass transition temperature ($T_g$) (**Fig. 2.5**). The $T_g$ of untreated glass is 809 K, but decreases up to 110 K after heat-treatment. The $T_g$ decreases continuously at low temperatures for samples foamed with 2-14 wt% $Na_2CO_3$. The samples with high amount of $Na_2CO_3$ (18-22 wt%) do not follow the decreasing $T_g$ trend at low temperatures, since they contain unreacted $Na_2CO_3$. This is also supported by DSC results which show endothermic peak originating from the decomposition of unreacted $Na_2CO_3$ (**Fig. 2.6**). $Na_2CO_3$ residuals are detected up to 1023 K for 22 wt% $Na_2CO_3$. It should be noted that only one

glass transition is detected with DSC, indicating the existence of only one amorphous phase. CRT panel glass re-melted at 1373 K with 22 wt% $Na_2CO_3$ has a $T_g$ of 716 K. This is 10-15 K higher than the foam glasses formed with 22wt% $Na_2CO_3$ at 1037-1173 K.

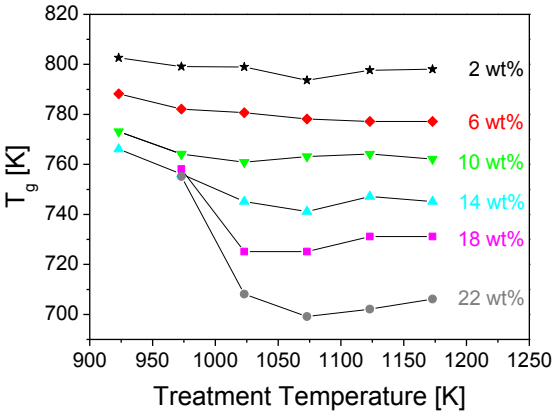


**Fig. 2.5** - Glass transition temperature ($T_g$) of foam glasses as a function of heat-treatment temperature. The samples were prepared with different concentrations of added $Na_2CO_3$ (see legend). $T_g$ is determined using DSC and the uncertainty is approximately ±3 K. In comparison, the $T_g$ of the untreated glass is 809 K, whereas the glass re-melted at 1373 K with 22 wt% $Na_2CO_3$ has a $T_g$ of 716 K. [Paper III]

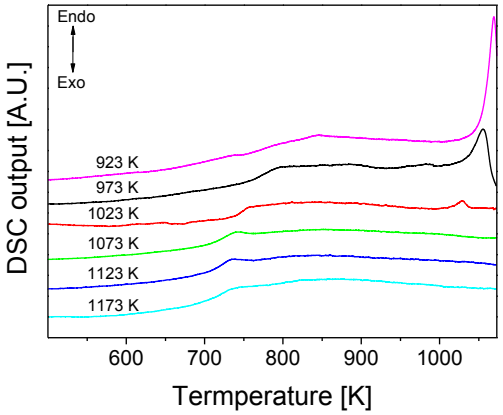


**Fig. 2.6** - DSC curves of foam glasses prepared with 22 wt% $Na_2CO_3$ by heat-treatment for 45 min at different temperatures (see legend). The curves are shifted vertically for clarity. [Paper III]

The possible reasons for the $T_g$ difference could be caused by crystallisation altering the glass composition. The crystal contains both network modifiers ($Na^+$, $Sr^{2+}$) and formers ($Si^{4+}$). The total non-bridging oxygen per tetrahedron (NBO/T) should decrease in the amorphous phase when crystalline $Na_2SrSi_2O_6$ is formed. Decreasing NBO/T normally result in increasing $T_g$. However, the $T_g$ of re-melted glass is higher than the foam glass with $Na_2SrSi_2O_6$ crystals. Studies on $Na_2O$ evaporation from $22Na_2O$-$78SiO_2$ glass (mol%) show that ~1±0.9 wt% loss of $Na_2O$ occurs at 1573 K after 60 min at an oxygen fugacity of $10^{-8}$ bar at 1 atm [30]. The re-melted glass is obtained at lower temperatures (1373 K) and higher oxygen fugacity and consists of ~21 mol% $Na_2O$ (if all $Na_2CO_3$ is decomposed). Since the evaporation increases with decreasing oxygen fugacity, evaporation of $Na_2O$ should be very limited when re-melting the CRT panel glass at 1373 K at 1 atm. In addition, no crystals are detected in the re-melted glass. Besides $Na_2SrSi_2O_5$ crystals, a few unidentified XRD peaks are found in the foam glass (**Fig. 2.4**) which indicates the presence of additional crystal phases which could alter the chemical composition.

The lower $T_g$ can also be associated to another phenomena. The reaction between glass melt and $Na_2CO_3$ occurs at the interface between glass melt and $Na_2CO_3$. The glass melt interface becomes enriched in $Na^+$ which subsequent diffuses into the glass melt. Since the $Na^+$ distribution is diffusion limited, $Na^+$ may not be homogenously distributed in the glass melt and some areas will have $Na^+$ rich domains. Consequently, the glass transition peak becomes broader at low treatment temperatures (923-1073 K, **Fig. 2.6**). The lower $T_g$ of foam glass compared to re-melted glass can be caused by the $Na^+$ rich domains which push the overall glass transition towards lower temperatures.

Isothermal treatment at 1073 K (5-45 min) shows that even after 5 min heat treatment the $T_g$ drops by 120 K compared to untreated glass ($T_g$ = 809 K). The initial drop show that the reaction between $Na_2CO_3$ and glass melt is fast. Increasing the duration further (5-45 min), the $T_g$ increases slightly again (**Fig. 2.7**). The XRD results indicate a slight growth crystallisation of $Na_2SrSi_2O_5$ which could lead to increase $T_g$, as discussed above. In addition, prolonged treatment time allows $Na^+$ to diffuse into a more homogenous distribution in the glass phase which results in an increase in the overall glass transition temperature.

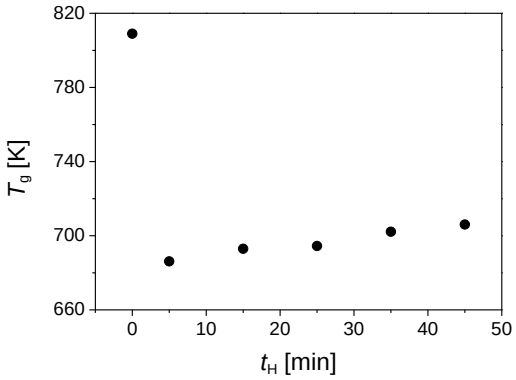


**Fig. 2.7** - Glass transition temperature ($T_g$) of foam glasses prepared with 22 wt% $Na_2CO_3$ prepared by heat-treatment at 1073 K for different treatment durations ($t_H$). Uncertainty of $T_g$ is approximately ±3 K. Untreated glass has a $T_g$ of 809 K. $T_g$ was determined from the first DSC upscan at the heating rate of 10 K/min. [Paper III]

## 2.4 Foaming Mechanism of Metal Carbonates

The thermal decomposition of pure alkali- and alkaline carbonates follows a so-called Congruent Dissociative Vaporization (CDV) mechanism. The solid carbonates dissociate first into gaseous products and the metal oxide subsequently condenses [29]. Simplifying the decomposition reaction by ignoring the evaporation-condensation step of metal oxide, the thermal decomposition of alkali- and alkaline carbonates follow this equilibrium:

$$M_xCO_3\ (s) \leftrightarrow M_xO\ (s) + CO_2\ (g) \qquad (\mathbf{2.3})$$

Pure $Na_2CO_3$ and $CaCO_3$ decompose around 1098 K and 873 K, respectively, when measured in air at 10 K/min. According to the equilibrium **Eq. (2.3)**, the formed $CO_2$ inhibits further thermal decomposition of $M_xCO_3$. When glass powder or melt are present, the decomposition is observed at much lower temperature, because the glass melt reacts with the metal carbonate. Verheijen [31] calls this reactive decomposition (or reactive calcination). Despite the important role of cullet in the glass industry, few studies on the reaction between metal carbonates and cullet exist [24,31-35]. König et al. [24] found through thermogravimetric analyses (TGA) in air atmosphere that $CaCO_3$ reacts readily with cullet well below the thermal decomposition temperature of $CaCO_3$. Similarly, Verheijen [31] shows with TGA in $CO_2$ atmosphere that $CaCO_3$ reactively decomposes with cullet ~160 K below its thermal decomposition temperature (1448 K). $Na_2CO_3$ decomposes likewise

reactively with cullet (**Fig. 2.2**) [PaperIII, PaperII], even in the preference of sand particles [33].

From the above results and explanations it can be deduced that the reaction kinetic of $Na_2CO_3$ and other metal carbonates is dependent on the contact surface area between the glass melt and the $M_xCO_3$ particles. This is already noticed before [24]. Several factors influence the contact area. Decreasing particle size [24], increases contact area. In addition, it is expected that a drop in melt viscosity induces a more effective contact area, since the gas formed at the melt/ $M_xCO_3$ interface is transported faster into the pore.

Furthermore, when heating above the melting temperature of $Na_2CO_3$ (1023 K), the contact area will be further increased. The $Na_2O$ formed from the reaction, is dissolved in the glass melt. Initially, the melt surface becomes enriched with $Na^+$. This enriched surface inhibits any further decomposition of $Na_2CO_3$ but the reaction continues once $Na^+$ poor glass melt appears at $Na_2CO_3$ particle. This occurs when the glass melt surface is depleted with $Na^+$ due to diffusion or when fresh glass melt appear at the $Na_2CO_3$ particle. Both melt flow and $Na^+$ diffusion accelerates with increasing temperature.

The reaction between metal carbonates and glass melt occurs fast. The formed $CO_2$ does not seem to decelerate the reactive decomposition. Therefore, the reactive decomposition is not controlled by slow equilibrium reaction but fast surface reaction. As a consequence, the gas formation is uncontrolled and bubbles expand very fast. The high pressure causes thinning and subsequent bursting of the cell walls and the foam glass ends up with large interconnected pores. Therefore, the density of foam glasses prepared with $CaCO_3$ [24,36-45], dolomite [40,45,46] or $Na_2CO_3$ [Paper I,43,44] rarely reaches below 0.2 g/cm$^3$ because they coalesce fast and attend high degree of open porosity [14,24,47] which ceases foam expansion. In other words, foaming agent following this reaction mechanisms result generally in foam densities above 0.2 g/cm$^3$ and tend to have open pore structure as the density drops to 0.2 g/cm$^3$.

Experiments show that an optimum $M_xCO_3$ concentration for low density foam glass exist. For $CaCO_3$ this is around 2-4wt% [24,38,43,45] and for $Na_2CO_3$ it is around 5 wt% [43] for glasses such as CRT panel glass [24,38], soda-lime-aluminosilicate [43] and float glass/fly ash [45]. If we assume all the gas formed becomes entrapped, 2 wt% $CaCO_3$ should produce foam glass with density of 0.06 g/cm3 (porosity of 98%). Small amount of $M_xCO_3$ can start to decompose before the glass sinters a closed structure [Paper I, Paper III], excessive amount should be added. However, when this is taken into account, the above mentioned concentration ranges still produces

excessive amount of gas at the heat-treatment temperature [PaperIII,24]. Hence, preferably lower $M_xCO_3$ concentrations and a glass type which does not react with $M_xCO_3$ should be used. It should be mentioned, that failure of using low $M_xCO_3$ concentrations could also be related to mixing. Mixing quality of glass powder and foaming is unfortunately not a topic that has been studied before.

## 2.5 Foaming Mechanism of Manganese Oxide

Metal oxides with multiple valence states are frequently used as foaming agent for glass melts. The metal oxide is either incorporated in virgin glass or added to powder mixture. $MnO_2$ is probably the most applied metal oxide as foaming agent. It is commonly used in combination with other foaming agents, such as $Si_3N_4$, C, SiC and TiN [16,18,21,22,48-50]. In the following, the reaction mechanism of manganese oxide is discussed in relation to foaming of glass melts.

### Thermal Characteristics of $MnO_2$ and $Mn_2O_3$

$MnO_2$ reduces to $Mn_2O_3$ at around 900 K ($T_{decomp,1}$) when β-$MnO_2$ is heated at 10 K/min in air atmosphere. This is observed with thermogravimetric analysis (TGA) by a distinct mass loss (**Fig. 2.8**). Increasing the temperature further, the sample mass stabilises again at 990 K. This indicates that the reduction of $MnO_2$ to $Mn_2O_3$ is completed. An additional reduction step ($Mn_2O_3 \rightarrow Mn_3O_4$) is observed above 1173 K [16, 51,52].

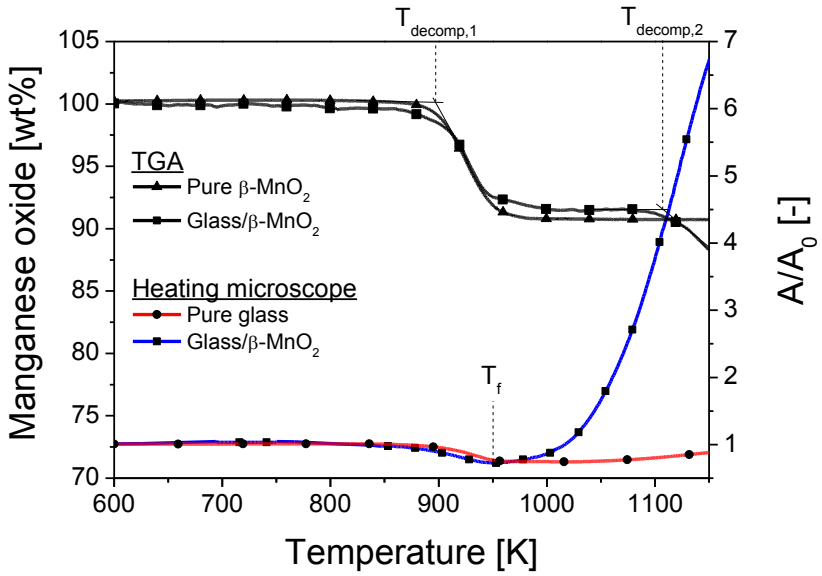


**Fig. 2.8 –** Mass loss of manganese oxide measured with thermogravimetric analysis (TGA) on pure β-$MnO_2$ and on CRT panel glass with 7wt% $MnO_2$ (left Y-axis). $MnO_2$ corresponds to 100% mass. Area ($A/A_0$) curves of pure CRT panel glass ($D_{90}$ = 32 µm) and of CRT panel glass with 7wt% $MnO_2$ (right Y-axis) were measured with heating microscope. TGA and heating microscope analysis were performed in air and at 10 K/min. [Paper I]

**Characteristics of Glass/$Mn_2O_3$**

When $MnO_2$ powder is mixed with CRT panel glass powder, $MnO_2$ reduces at the same temperature and follows roughly the same mass loss kinetic as pure $MnO_2$. Hence, no detectable interaction between CRT panel glass and $MnO_2$ occurs in the temperature range of 830 to 990 K. At elevated temperatures ($T_{decomp,2}$) a distinct mass loss is observed (**Fig. 2.8**). This occurs because the glass melt causes reduction of $Mn_2O_3$. The glass melt destabilises $Mn_2O_3$, allowing reduction of $Mn_2O_3$ below 1173 K. Redox studies of $Mn^{2+}/Mn^{3+}$ in glass melts at high temperatures (T ≈ 1240–1550 K) show that $Mn^{2+}$ is the dominating oxidation state [53]. If we extrapolate those results to our lowest heat-treatment temperature ($T$ = 1063 K), we get $Mn^{2+}/Mn^{3+} \approx 2$. This indicates that the presence of $Mn^{2+}$ is favourable in the CRT panel glass melt at treatment temperature.

The XRD results show that the $Mn_2O_3$ crystals are gradually disappearing in the foam glass with increasing temperature and extended time (**Fig. 2.9**). This shows that $Mn_2O_3$ slowly dissolves in the glass melt. The local redox

potential causes reduction of the dissolved $Mn^{3+}$ to $Mn^{2+}$ and formation of $O_2$ according to the equilibrium:

$$2Mn^{3+}\ (melt) + O^{2-}\ (melt) \leftrightarrow 2Mn^{2+}\ (melt) + ½O_2\ (gas) \qquad (\mathbf{2.4})$$

The diffusion of $Mn^{2+}$ and $O_2$ away from the $Mn_2O_3$ particle enhances further reduction of $Mn^{3+}$ according to the equilibrium **Eq.** (**2.4**). The dissolution of $Mn_2O_3$ particles is diffusion-limited and accelerates at higher temperatures (**Fig. 2.9a** and **2.9b**) when the melt viscosity decreases. Hence, the reduction of $Mn^{3+}$ is not only coupled to reduction potential but also to dissolution and diffusion kinetics.

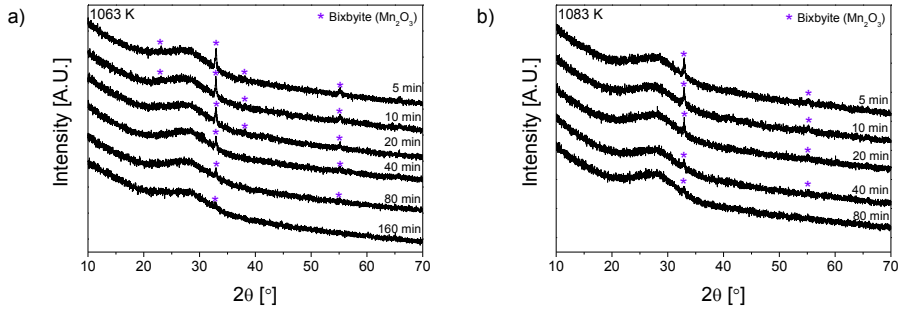


**Fig. 2.9 –** XRD patterns of crushed foam glasses prepared at a) 1063 K and b) 1083 K at different treatment times (see legend). The spectra are shifted vertically for clarity. The JCPDS card number 01-089-2809 is used to identify $Mn_2O_3$. [Paper I]

**Foaming Mechanism**

Waste glasses [54] and natural basalt glasses [55] can foam at elevated temperature without adding additional foaming agents. As shown in **Fig. 2.8**, CRT panel glass powder mainly densifies when heated but foams when $MnO_2$ is present. Since the $MnO_2$ decomposes during the glass sintering (**Fig. 2.8**), a major part of the $O_2$ generated from $MnO_2$ reduction escapes the glass body. As shown in **Fig. 2.8**, the foaming begins at 950 K ($T_f$) before the reduction of $Mn_2O_3$ is detected at 1100 K ($T_{decomp,2}$). This indicates that a small amount of $O_2$ becomes entrapped in the sintered body. At elevated temperatures ($T > T_{foam}$) the $O_2$ pressure in the pores increases and causes initial expansion.

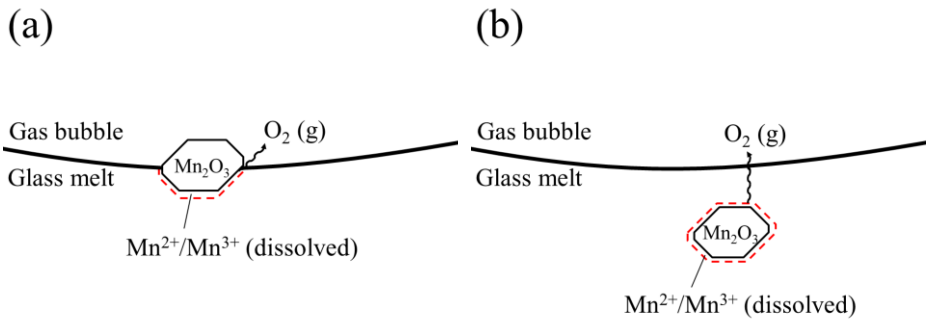


**Fig. 2.9 –** a) The $Mn_2O_3$ particles are partially immersed in the glass melt (short treatment times). The $O_2$ formed from the reduction of $Mn^{3+}$ diffuses to the existing bubble. b) The $Mn_2O_3$ particles are completely immersed in the glass melt (long treatment times). The formed $O_2$ diffuses to existing pores or nucleates new pores in the glass melt. [Paper I]

If $Mn_2O_3$ particles are located on the pore wall or partially immersed in the glass melt, the formed $O_2$ at the glass-$Mn_2O_3$ interface would not lead to any new pores but increase the pressure in existing pores (**Fig. 2.9a**). With time, $Mn_2O_3$ particles become completely immersed in the glass melt. $O_2$ formed at the surface of $Mn_2O_3$ particles can diffuse to the existing pores, increasing the pressure in pore (**Fig. 2.9b**). If the $O_2$ formation is faster than the diffusion limited removal rate, the glass melt becomes supersaturated. As a consequence, homogeneous or heterogeneous nucleation of closed pores (bubbles) can occur. Since $Mn_2O_3$ particles are present, bubble nucleation will preferably occur at the $Mn_2O_3$ surface. It is not possible to find any crystals located at the pore wall with SEM. However, high Mn concentrations combined with low Si concentrations are found as black spots in the glass matrix (**Fig. 2.10**). This confirms that manganese oxide is immersed in the glass melt.

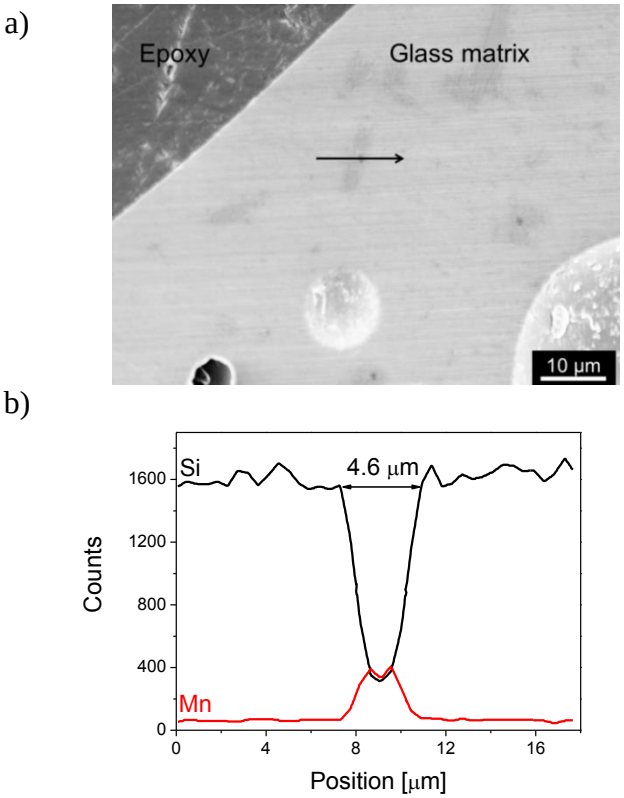


**Fig. 2.10 –** a) SEM image and b) EDX line scan of foam glass. The arrow shows the position and direction of the EDX line scan shown in b). The foam glass is prepared at 1063 K for 80 min. [Paper I]

During the foaming process, the pores become open, allowing the exchange of $O_2$ with air atmosphere. Since the reduction potential increases with decreasing oxygen pressure **Eq. (2.2)**, a further reduction of dissolved $Mn^{3+}$ can occur, resulting in nucleation and growth of new bubbles.

Based on valence state (Z) and ionic radii (r) of manganese with different coordination number (CN) from Shannon [56], the field strength (FS = $Z/r^2$) calculations indicate that $Mn^{2+}$ should be classified as network modifier (FS = 0.37–0.50, CN = 4–8) and $Mn^{3+}$ as an intermediate (FS = 0.81, CN = 5 or 6). The increased dissolution of $Mn^{2+}$ could therefore lead to depolymerisation of the [$SiO_4$] network. It was shown earlier that the $T_g$ drop depends on $Na_2CO_3$ concentration, temperature and time (**Fig. 2.5** and **2.7**). The effect of $Mn^{2+}/Mn^{3+}$ on $T_g$ is much weaker than alkali oxides and no significant time or temperature dependent effect on $T_g$ is found.

## 2.6 Summary

Based on experimental studies with $Na_2CO_3$ and $MnO_2$ as foaming agents and literature, the reaction mechanism of metal carbonates and metal oxides must be treated separately.

The metal carbonates are characterised by a surface reaction between glass melt and the metal carbonate. The surface reaction is fast and the $CO_2$ formation does not seem to inhibit any further decomposition. The $CO_2$ is therefore produced uninhibited. The surface reaction occurs around or even below the glass transition temperature. Therefore, the metal carbonates release gas before the glass sinters a closed body. Hence, excess metal carbonates are needed for foaming low density foam glass [Paper III, 1, 24]. This on the other hand can lead to open porosity. I discussed, that the melt surface available for reaction is dependent on viscosity and $Na^+$ diffusion. Metal carbonates with slowly diffusing cations (e.g. $Sr^{2+}$, $Ba^{2+}$) should limit the overall reaction kinetic.

The metal oxides first dissolves in the glass melt and reduces according to the equilibrium chemistry for glass melts. Consequently the gas release kinetics is more controlled. In addition, the metal oxides become incorporated into the glass melt. Any gas formed in the glass melt will diffuse to the bubble. Hence, the gas formation is more controlled and foam glasses with more homogenous pore structure can be achieved.

# 3. Foam Dynamics

The growth of foam glass is important process to understand in order to develop low density foam glass. The open pores are formed when pore walls between the pores breaks. There are no studies on the pore wall stability of foam glass, but there exist several studies on vertical molten glass films [57-60] and single melt bubbles [61,62].

Since we wish the foam glasses to have closed pores, the growth process should be compared to the formation of open pores. Few systematic studies demonstrate how closed porosity can be controlled in foam glass by varying different process parameters [18,55,63].

In this chapter, the foam expansion and coalescence are compared. 7 wt% $MnO_2$ is used as to foam CRT panel glass at various times and temperature. The reader is referred to Sec. 2.5 for the reaction mechanism of this system **Sec. 2.5**.

## 3.1 Foam Growth

The powder mixtures were heat-treated at 1063 K and 1083 K at different time intervals (5-160 min). Foam density ($\rho_{foam}$) decreases exponentially with time (**Fig. 3.1)**. The exponential foam density trend agrees well with foam glasses obtained with AlN at 1233 K and 1293 K [64]. On the other hand, CRT panel glass foamed with 3 wt% $CaCO_3$ did not reveal any significant change of foam density (relative density varied ± 0.1) for different holding times between 5-60 min at 1023 K [38]. König et al [18] foamed CRT panel glass with 1 wt% C and 5.4 wt% $MnO_2$. The foam density decreased slightly when foaming at 1053 K for 5-60 min, whereas heat-treatment at 1073 and 1093 K increased the foam density with time. König et al [18] used much smaller particles than in my studies. Therefore, the gas formation rate is higher since larger contact area between melt and $Mn_2O_3$ exist. In this study, the rate is low and a decrease in foam density can therefore be observed.

At a higher treatment temperature the dissolution rate of $Mn_2O_3$ and the gas formation rate are higher, since the melt viscosity is lower. Together with thermal pressure increase, these factors contribute to faster foam growth at higher temperatures.

Initially the redox reaction **Eq.** (**2.4**) is far from equilibrium and the gas formation is fast. In addition, the dissolution rate is also expected to be faster in the beginning, since the total particle surface in contact with the glass melt is greater in the beginning if the particles are immersed. Since the amount of crystalline $Mn_2O_3$ decreases with treatment time, the total particle surface

area decreases and, hence, the dissolution rate decreases. As dissolution rate decreases and $Mn^{2+}/Mn^{3+}$ ratio approaches equilibrium state, the gas formation rate diminishes with time.

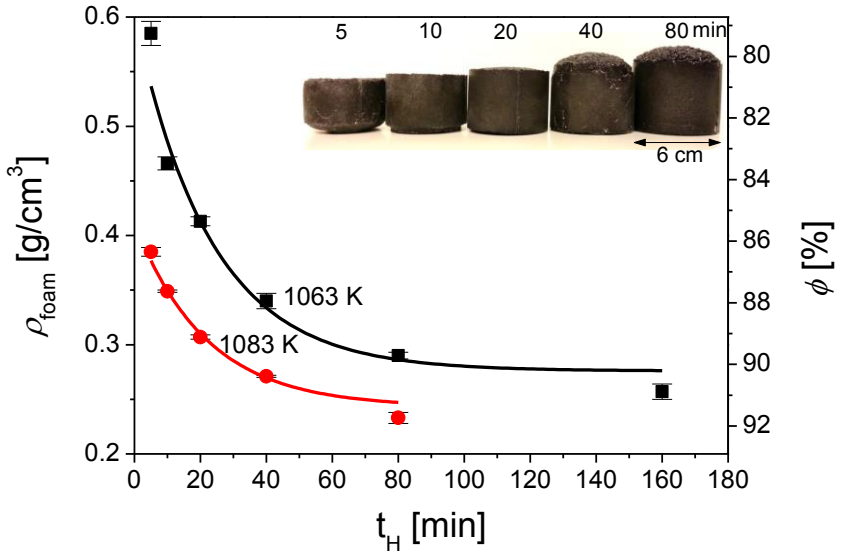


**Fig. 3.1 –** Foam density ($\rho_{foam}$) of the foam glasses prepared at different treatment times ($t_H$) at either 1063 K or 1083 K (see legend). The lines are exponential decay function fitted to data. The error bars represent uncertainties of the foam volume determination. The inset shows the photographed foam glasses formed at 1083 K for different $t_H$ (5–80 min). [Paper I]

### 3.2 Formation of Percolated Foams

Simultaneously with foam growth, the pores coalesce. At some critical thickness the pore wall ruptures and the pores sharing the pore wall merge together (coalesce). There are two processes causing pore wall thinning. Melt drains from the pores into the struts and pore growth cause wall stretching, resulting in thinner pore walls. The wall breaking is reflected in the degree of closed porosity ($\varphi_{CP}$).

Initially (0–10 min), the pores are closed and surrounding atmosphere cannot penetrate into the foam (**Fig. 3.2**). Within short treatment time ($t_H$ > 20 min at 1063K) the foam becomes percolated ($\varphi_{CP}$ < 20%). When treatment temperature is raised to 1083 K, the percolation time decreases. Two factors cause higher coalescence rate: First, increasing temperature accelerates the gas formation rate. Second, the pores will grow due to thermal expansion of the gas and the lower melt viscosity. The drainage time

scale (167 min at $10^6$ Pa s) [65] is insignificant in comparison to our experimental time scale (5-160 min).

It is interesting to see that after very long treatment time (e.g. $t_H$ >80 min at 1063 K), the closed porosity increases slightly again. This happens when new closed pores are nucleated in the struts or in the pore walls of larger pores.

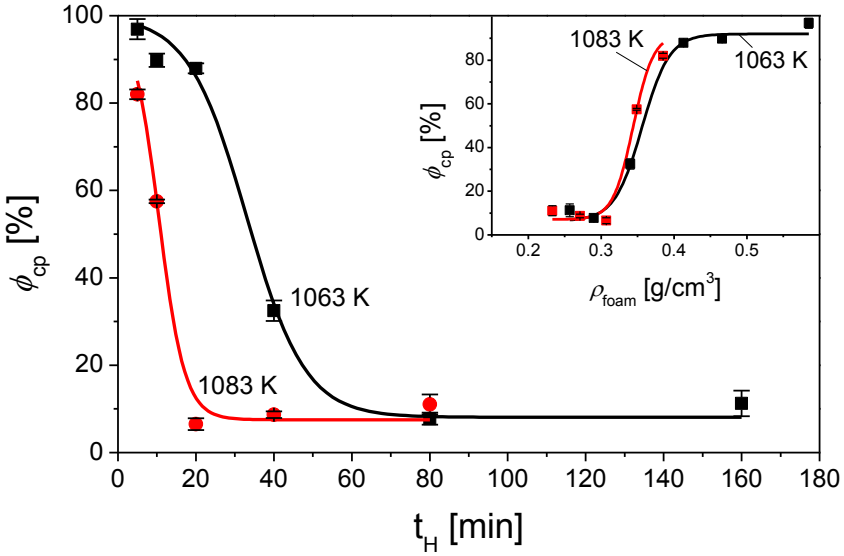


**Fig. 3.2 –** The closed porosity ($\varphi_{cp}$) of the foam glasses formed at different treatment times ($t_H$) at either 1063 K or 1083 K (see legend). The volume of the analysed samples is 34–36 cm$^3$. The closed porosity is calculated according to **Eq. (2.2)**. The error bars represent combined standard deviations of $\rho_{pow}$, $\rho_{foam}$ and $\rho_{skel}$. The lines are sigmoidal Boltzmann functions fitted to the data. The inset shows $\varphi_{cp}$ as a function of foam density ($\rho_{foam}$). [Paper I]

The percolation threshold ($\varphi_{cp}$ < 50%) is reached when the foam reaches a density around 0.35–0.40 g/cm$^3$ (**inset in Fig. 3.2**). In comparison, the foaming of CRT panel glass with $MnO_2$/C using smaller particle size ($D_{90}$ = 14.8 μm) can achieve lower density (<0.20 g/cm$^3$) and a high degree of closed porosity [18]. In this study, we use larger particle size of $MnO_2$ ($D_{90}$ = 40 μm). The larger particle size could cause faster coalescence.

The critical thickness of pore wall rupture is calculated to be in the range of 1-20 nm [62]. However, particles in foam suspension can destabilise pore walls [66] by increasing the critical thickness of rupture if the particle is partially or completely immersed into the glass melt [67]. As shown in **Fig.**

**2.9**, $Mn_2O_3$ crystals are immersed in the glass melt. Additional particles identified in the glass matrix have high Si content and low content of other cations (**Fig. 3.2**). Cristobalite is a $SiO_2$ polymorph formed at 1048–1373 K in float glass [68] and borosilicate glass [69]. The foam glasses in this study are prepared at 1063 and 1083 K. Therefore, the Si rich particles are probably cristobalite crystals. Both $Mn_2O_3$ and cristobalite could have a destabilising effect on the pore wall.

As discussed in Sec. 2, the $Na_2O$ becomes heterogeneously incorporated into the glass melt. The EDX line scans show small concentration gradients of manganese in the glass melt. This strongly indicates that $Mn^{2+}/Mn^{3+}$ is heterogeneously distributed in the glass melt (**Fig. 3.3c**).

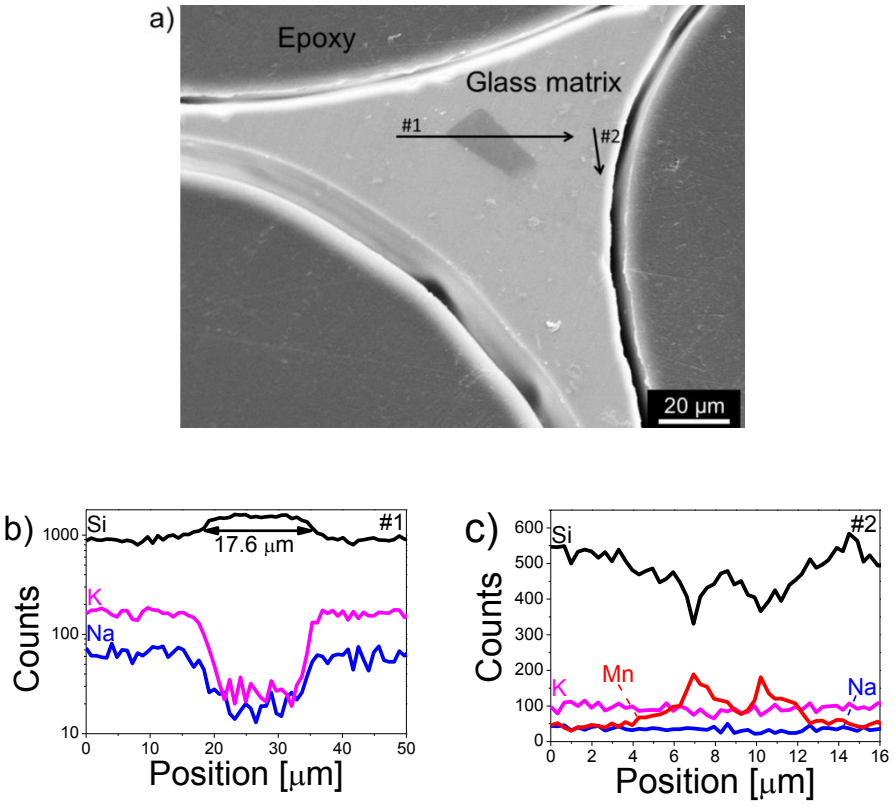


**Fig. 3.3 –** a) SEM image of a glass strut and epoxy filled pores. The arrows show the positions and directions of the EDX line scans: b) Scan #1 shows Si rich phase, c) Scan #2 shows inhomogeneous incorporation of Mn. The foam glass is prepared at 1083 K for 20 min. Notice the log scale on the Y-axis in b). [Paper I]

Initially after the coalescence of two pores, the new pore is irregularly shaped. The new pore changes into a spherical shape again, since it has a lower surface energy. However, the shape transformation is kinetically dependent on the melt viscosity and since the viscosity is high, the time required for the pore to return to spherical shape increases with pore size. Simultaneously, the coalescence rate is fast and the pore coalesces with near-by pores before gaining spherical shape. Thereby, the pores become increasingly irregular in shape with prolonged treatment (**Fig. 3.4**) and the number of connections with neighbouring pores increases (**Fig. 3.4f**).

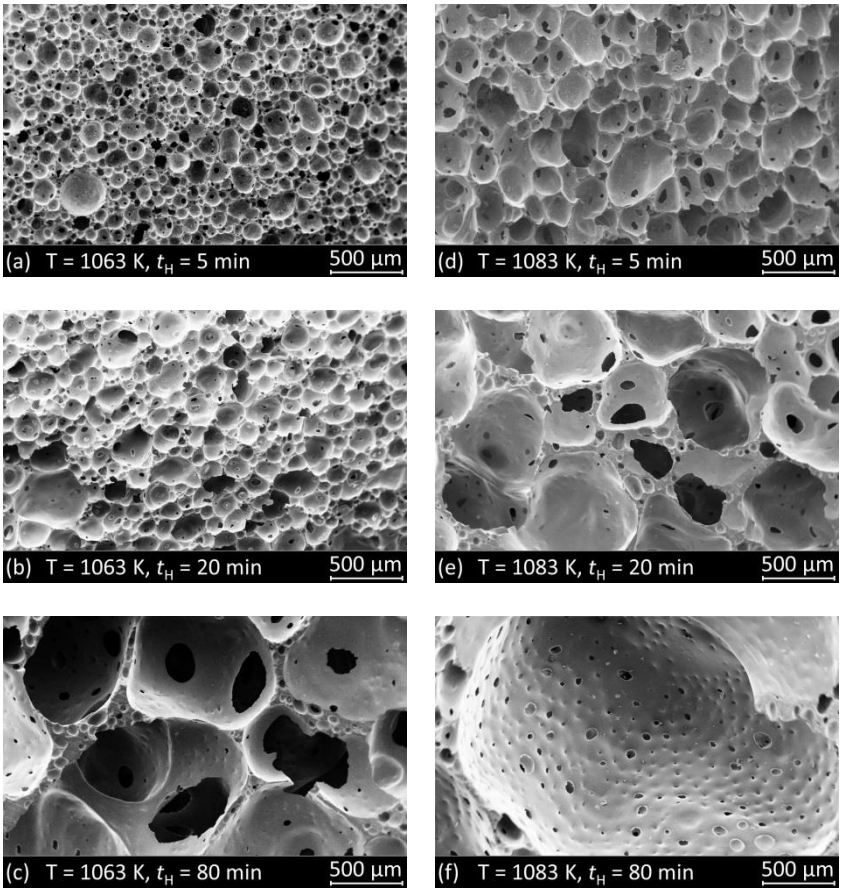


**Fig. 3.4 –** SEM images of the foam glasses prepared from CRT panel glass and 7 wt% $MnO_2$ foamed at **a–c)** 1063 K and **d–f)** 1083 K for different treatment times (see legends). [Paper I]

The pores evolve in a bimodal pore size distribution with increasing $t_H$ (**Figs. 3.4d-f**). Two possible mechanisms explain this. First, larger pores have a higher surface area and more oxygen will diffuse into the pores. Hence, large pores will grow faster. Second, the pore size will increase due to coalescence and gas formation, meanwhile nucleation and growth of new pores will promote the pore population at the lower size part of the pore size distribution.

Another important consequence of coalescence is a decreasing number of pores. The pore number density is shown in **Fig. 3.5**, where the bubble number density ($N_A$) is corrected for foam growth by multiplying the apparent bubble number density ($N$) with the volume ratio ($V_0/V_i$ ). Here, $V_0$ is the volume of the foam with the highest density and $V_i$ is the respective foam volume. The $N_A$ decreases exponentially with treatment time and with increasing temperature. Decrease of $N_A$ can be caused by inter-bubble diffusion (Ostwald ripening) and coalescence [70]. Ostwald ripening is the diffusion of gas from closed pores with high pressure (small pores) to closed pores with low pressure (large pores).

The glass melt is saturated with $O_2$ formed from the $Mn^{3+}$ reduction. Therefore, there is a net diffusion of $O_2$ into every pore. Since, Ostwald ripening requires a diffusion gradient from small to large pores, it cannot take place and coalescence must be causing the exponential decrease of $N_A$. The $N_A$ becomes smaller at higher temperatures 1083 K (**Fig. 3.5**). The increase temperature expands the pores due to pressure increase and decrease viscosity. Both factors increases cell wall thinning and coalescence rate. At long $t_H$ (40–80 min) the $N_A$ seems to reach a steady state or even a slight increase. Since the pores coalesce at all time, the steady-state trend of $N_A$ must be influenced by the formation of new bubbles (nucleation). The SEM image (**Fig. 3.2f**) indicates that new pores are formed and grown in the strut and cell wall.

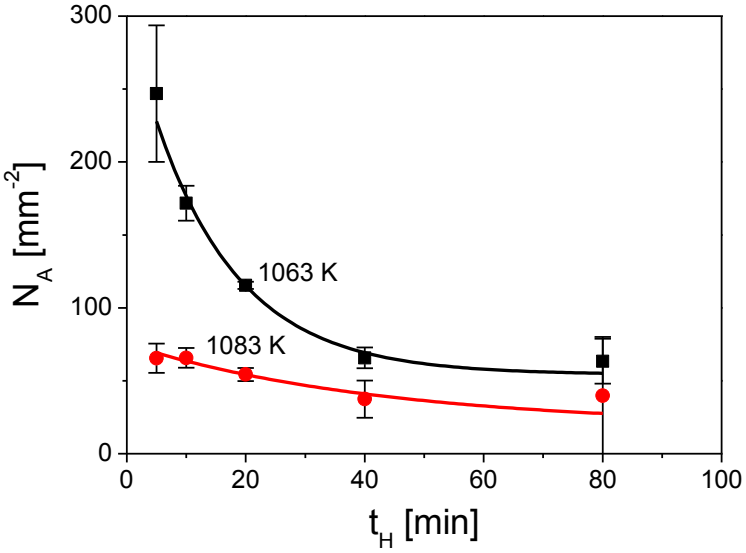


**Fig. 3.5 –** The number of pores per image area ($N_A$) for samples prepared at different treatment times ($t_H$) and different temperatures (see legend). $N_A$ is obtained from at least three SEM images of the epoxy mounted foam glasses. The error bars represent the combined uncertainty of the pore counting ($N$) and the density ($\rho_{foam}$) measurement. [Paper I]

### 3.3 Growth of Percolated Foam

Despite the pores becoming open and connected, the foam continues to grow (compare **Fig. 3.1** and **Fig. 3.2**). Two possible reasons can cause foam growth during percolation stage ($\varphi_{cp}$<20%). First, the nucleation and growth of new bubbles will cause foam growth. However, the bubbles will eventually coalesce with large pores (as indicated in **Fig. 3.2f**) which then halts the pore growth. Second, the open pores can continue to grow, if the pores located at the outer sample surface are closed. However, when the pore wall ruptures, the subsequent closure is slow due to the high melt viscosity. Therefore, bubble nucleation and growth is the major cause of foam growth during percolation stage.

During percolation stage ($\varphi_{cp}$<20%) the pore size continues to increase (**Fig. 3.4**). Both pore growth and coalescence can cause larger average pore size. Growth of open pores, as discussed above, is presumed to be negligible. Therefore, the increase pore size is caused by coalescence.

## 3.4 Summary

The growth mechanism of foam glass and the formation of open pores are discussed. The foam grows exponentially with time. Despite the foams become percolated the foams continue to grow slightly. This was attributed to nucleation and growth of new bubbles. We show in addition, that $Mn^{2+}/Mn^{3+}$ is incorporated heterogeneously in the glass melt.

# 4. Foaming Ability

The foaming process is controlled by many parameters and optimisation is very time consuming. The most influential parameter is temperature. Altering the temperature leads to changes in melt viscosity, gas pressure, gas formation rate, coalescence rate and crystallisation kinetics. Several experimental studies show that apparent density reaches a minimum when the treatment temperature is varied [PaperIII,45,46]. This indicates that foam expansion occurs at some ideal viscosity range. This chapter focuses on developing temperature and viscosity criteria for optimal foaming of glass melt.

### 4.1 Viscosity limit

We compare the foaming behaviour of different glasses with commercial relevant compositions (Labware glass, E-glass, soda-lime-silica glass, CRT panel glass, **Table 4.1**). Melt viscosity (or isokom temperature) is varied while treatment time, particle size, sample size, compaction pressure, type and concentration of foaming agent are kept constant. The foaming is induced by adding $CaCO_3$ as foaming agent which decomposes into CaO and $CO_2$. The foaming behaviour is discussed in terms of surface tension and glass stability.

**Table 4.1 –** Chemical composition glass powder. Besides the reported oxides, Labware and E-glass contain $B_2O_3$.

| Oxide | Chemical composition [wt%] | | | |
|---|---|---|---|---|
| | Labware | E-glass | CRT panel | SLS |
| $SiO_2$ | 80 | 53 | 61 | 73 |
| $Al_2O_3$ | 2.6 | 14.0 | 1.9 | |
| $Fe_2O_3$ | 0.9 | 1.0 | 0.5 | 0.5 |
| $Na_2O$ | 3.9 | 0.9 | 7.3 | 15.6 |
| $K_2O$ | 0.1 | 0.1 | 7.5 | |
| CaO | 0.4 | 22.9 | 0.1 | 9.2 |
| SrO | | 0.2 | 8.8 | |
| BaO | | 0.1 | 10.1 | |
| $ZrO_2$ | | | 1.4 | |
| ZnO | | | 0.5 | |

**Viscosity measurement**

The high viscosity of glasses melts are measured with micro penetration method on a Vis 405 viscometer (Bähr Thermoanalyse GmbH) and the viscosities above liquidus temperature were obtained with a Rheolab MC1 rotation viscometer (Physica Messtechnik GmbH). Four different glasses were studied: Labware glass (Simax) from laboratory, E-glass, CRT panel glass and soda-lime-silica glass. The viscosity data were fitted with the MYEGA model [71] Eq. (**4.1**).

$$\log \eta = \log \eta_\infty + (12 - \log \eta_\infty)\frac{T_{g,vis}}{T}\exp\left[\left(\frac{m}{12-\log \eta_\infty}\right)\left(\frac{T_{g,vis}}{T} - 1\right)\right] \quad (\mathbf{4.1})$$

where $\eta$ is the glass melt viscosity, $\eta_\infty$ is the viscosity at infinite high temperature, $T_{g,vis}$ is the glass transition temperature, $T$ is the measured temperature and $m$ is the fragility.

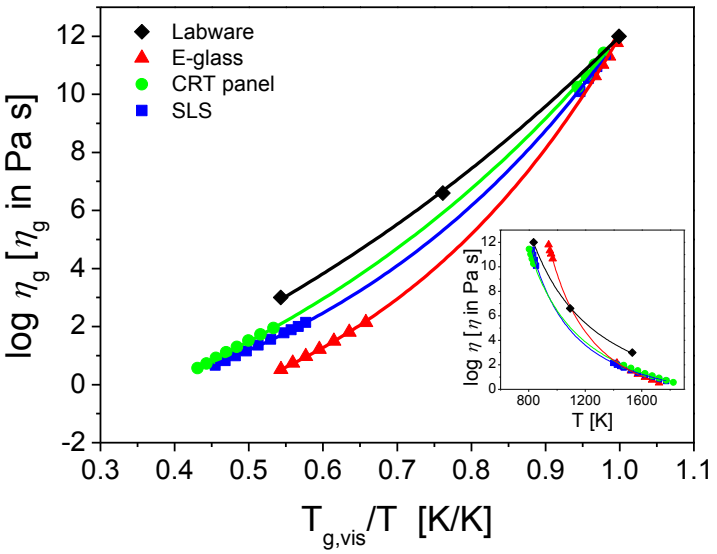


**Fig. 4.1** – Angell viscosity plot of different glasses (see legend) showing logarithmic viscosity (log $\eta_g$) as a function of inverse temperature ($T$) scaled to the glass transition temperature ($T_{g,vis}$) obtained from fitting the viscosity data to MYEGA equation. The viscosity error at high temperature (measured with concentric cylinder) and at low temperature (measured with ball penetration) is $\eta$ = ±0.13 Pa s and $\Delta\log_{10}\eta$ = 0.24 ($\eta$ in Pa s), respectively. Data for Labware glass are from manufacture. The solid lines represent fits using the MYEGA equation (4.1).

It was not possible to measure viscosity of labware glass at high temperatures (1773 K), since the viscosity was too high to efficiently remove the bubbles. Instead, viscosity data from the manufacturer (Simax, France) was used to fit the whole temperature range by treating log $\eta_\infty$ as constant in the MYEGA equation. The log $\eta_\infty$ was fixed as -2.93, since silicate melts tend to have this common log $\eta_\infty$ value [72]. The viscosity data can be found in **Fig. 4.1** and the resulting fitting parameters can be found in **Table 4.2**.

**Table 4.2 –** Density ($\rho$) and MYEGA fitting parameters ($T_{g,visc}$, $m$, log $\eta_\infty$). $T_{g,visc}$ is the glass transition temperature at $10^{12}$ Pa s, $m$ is the liquid fragility index and log $\eta_\infty$ is the logarithmic viscosity at infinite high temperature.

| Glass | $\rho$ [g/cm$^3$] | $T_{g,visc}$ [K] | $m$ [-] | log $\eta_\infty$ [Pa s] |
|---|---|---|---|---|
| Labware | 2.2248 ± 0.0003 | 832 ± 3 | 25.5 ± 0.5 | -2.93* |
| E-glass | 2.6317 ± 0.0005 | 936.5 ± 0.6 | 44.2 ± 0.8 | -2.7 ± 0.2 |
| CRT panel | 2.7730 ± 0.0009 | 786 ± 1 | 30.7 ± 0.9 | -2.9 ± 0.3 |
| SLS | 2.4803 ± 0.0017 | 806.6 ± 0.7 | 36.2 ± 0.6 | -2.0 ± 0.1 |

* *Fixed fitting parameter*

Powdered glass with similar particle size (**Fig. 4.2**) with 2wt% $CaCO_3$ are heat-treated for 30 min at different viscosities ($10^3$–$10^{10}$ Pa s). The isokom treatment temperatures ($T_H$) were calculated with an iterative solution of Lambert-W-function [73] using the obtained MYEGA fitting parameters. The calculated $T_H$ are found in **Table 4.3.**

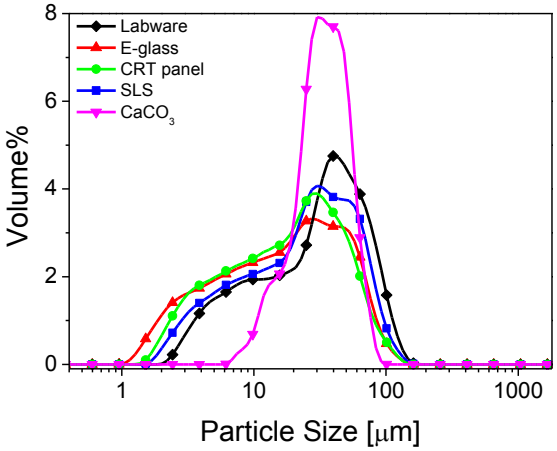


**Fig. 4.**2 – Particle size distribution of $CaCO_3$ (foaming agent) and different glass powder (see labels).

**Table 4.3** – Isokom heat-treatment temperatures ($T_H$) and corresponding logarithmic viscosity ($\eta_g$) of the glass melts. Temperature values were calculated with MYEGA viscosity model [73] using the fitting parameters from Table 4.2.

| Glass | log $\eta_g$ [Pa s] | | | | | | | |
|---|---|---|---|---|---|---|---|---|
| | 3 | 4 | 5 | 6 | 7 | 8 | 9 | 10 |
| | $T_H$ [K] | | | | | | | |
| Labware | 1521 | 1362 | 1241 | 1146 | 1070 | 1006 | 953 | 907 |
| E-glass | 1334 | 1248 | 1182 | 1128 | 1083 | 1045 | 1012 | 984 |
| CRT panel | 1302 | 1186 | 1097 | 1026 | 968 | 920 | 879 | 844 |
| SLS | 1268 | 1160 | 1080 | 1017 | 966 | 924 | 888 | 857 |

**Crystallisation**

Cristobalite crystals are formed in labware glass after heat-treatment in the range of 1070–1241 K ($10^5$–$10^7$ Pa s) and quartz after foaming at 1146 K and 1241 K (**Fig. 4.3a**). This is in accordance with similar borosilicate compositions which crystallise cristobalite in the temperature range of 973–1273 K [74,75].

E-glass crystallises wollastonite ($CaSiO_3$) and anorthite ($CaAl_2Si_2O_8$) in the temperature range of 1083–1248 K ($10^4$–$10^7$ Pa s) and quartz in the temperature range of 1128–1248 K (**Fig. 4.3b**). Martin et al. [76] also find wollastonite in similar E-glass composition between 1173–1373 K. Müller et al [77] found in a similar glass composition (38CaO $4.7Al_2O_3$ $7.3B_2O_3$ $50SiO_2$) wollastonite and anorthite crystals after heat-treatment in the same temperature range.

Foamed CRT panel glass hardly crystallise in a broad temperature range (**Fig. 4.3c**), even when $CaCO_3$ is added as foaming agent. This is in agreement with earlier studies on foaming of CRT panel glass using $CaCO_3$ [24,36] or $MnO_2$ [PaperIII,18] as foaming agent. The residual CaO is dissolved into the glass melt. Furthermore, the $CaCO_3$ is no longer detectable with XRD above 1097 K, indicating that $CaCO_3$ is completely decomposed.

Heat-treated soda-lime-silica (SLS) glass crystallise cristobalite and quartz between 966–1160 K ($10^4$–$10^7$ Pa s) and devitrite at 1080 K and 1160 K ($10^5$–$10^4$ Pa s), see **Fig. 4.3d**. Crystallisation studies on bulk float glasses show that cristobalite is formed at 938–1198 K and devitrite at 1023–1198 K in air atmosphere [68,78]. Prado et al. [79] crystallises, devitrite, cristobalite quartz and wollastonite in soda-lime-silica glass powder at 1123 K for 14 h and at 1173 K for 6 h.

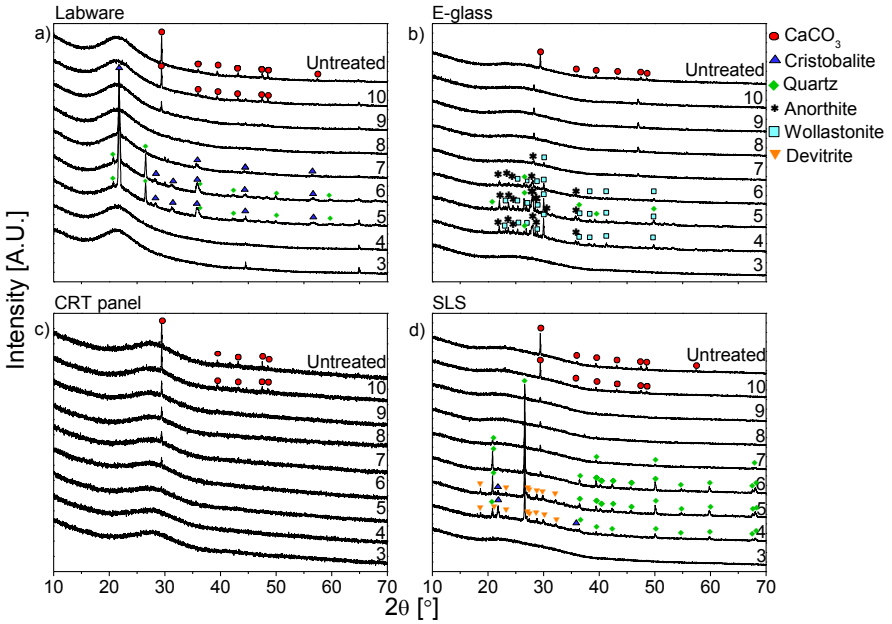


**Fig. 4.3** – XRD patterns of untreated glass powder and glasses heat-treated for 30 min at different viscosities (log $\eta_g$ = 3–10, see legend). The patterns have been vertically shifted for clarity.

**Isokom foaming**

Simultaneously with glass sintering $CaCO_3$ decomposes, resulting in CaO and $CO_2$. The decomposition occurs due to thermal instability above 950 K and due to reaction with the glass melt [24,31,32]. If the decomposition happens while the glass sinters closed cavities, the resulting $CO_2$ gas will form bubbles in the sintered glass melt, resulting in foaming.

The effect of heat-treatment at isokom temperature on apparent density is shown in **Fig. 4.4**. As the viscosity is decreased ($10^{10}$–$10^8$ Pa s) the glass melt densify, reaching a density maximum at $10^8$ Pa s for CRT panel and SLS glass and $10^7$ Pa s for Labware and E-glass ($\eta_{max}$ = $10^7$–$10^8$ Pa s). At lower viscosity the glass melt foams. The sintering rate increases with lower viscosity and below $\eta_{min}$ the sintering rate becomes fast enough to entrap the $CO_2$ gas before it escapes. A minimum in density is reached at $10^5$ Pa s for CRT panel and labware glass and $10^{5.5}$-$10^6$ Pa s for SLS glass. At even lower viscosities ($\eta_g$ < $10^5$ Pa s) the apparent density increases again. The low viscosity accelerates pore wall thinning and coalescence will occur fast. Hence, foam collapsing occurs. E-glass behaves differently by not showing any minimum. Instead, the density decreases continuously below $10^7$ Pa s with decreasing viscosity.

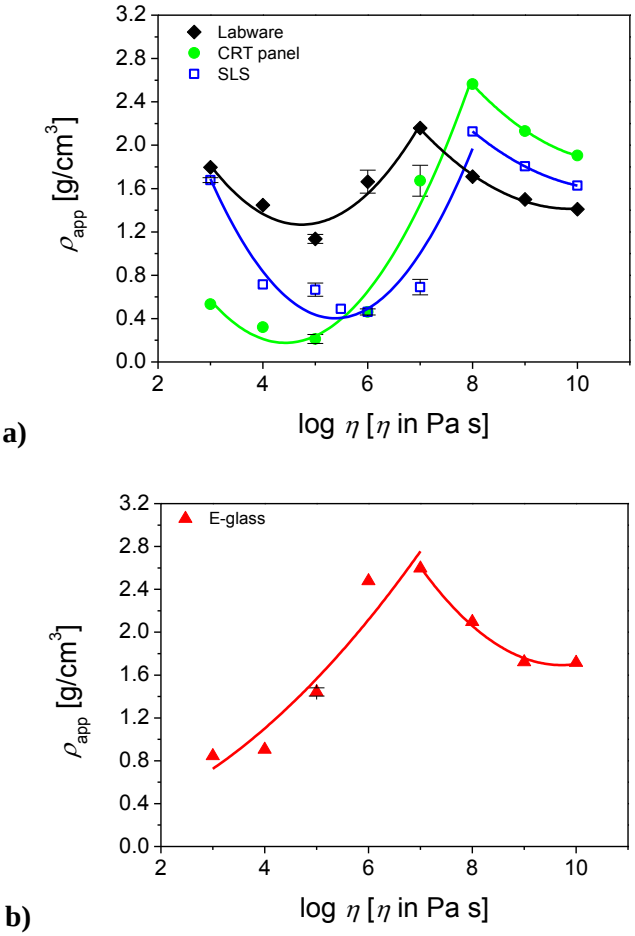


**Fig. 4.4** – Apparent densities ($\rho_{app}$) of glasses sintered and foamed by heat-treating isothermally for 30 min at different melt viscosities (log $\eta$). a) shows CRT panel glass, soda-lime-silica (SLS) glass and labware glass and b) shows E-glass. The error bars represent standard deviation of three replicates. The solid lines are guides for the eye.

**Effect of surface tension**

**Table 4.4** shows the calculated surface tension ($\gamma$) at different temperatures. The calculated $\gamma$ values of SLS and CRT panel glass are in accordance with experimental values [80,81]. In comparison with the other glasses, the E-glass has a higher surface tension (343–386 mN/m). Kraxner et al [82] measured surface tension using both drop profile analysis and Dorsey's method on 27CaO $4.9B_2O_3$ $9.5Al_2O_3$ $59SiO_2$ (mol%). They attainted 276 mN/m (drop profile analysis) and 288 mN/m (Dorsey's

method) for the glass composition. The models used for calculated surface tension are not based on calcium aluminoborosilcate compositions [83, 85,84]. Hence, Kraxner et al's [82] measurement seems to be the best approximation.

**Table 4.4** – Calculated surface tension ($\gamma$) of glass melts at different temperatures. Different models are applied [80,83-85]. The $B_2O_3$ content for labware and E-glass is assumed to be: $X_{B_2O_3} = 100\% - \sum X_i$, where $X_i$ is the content of individual oxides in wt% quantified with XRF.

| Glass | $\gamma$ [mN/m] | | | |
|---|---|---|---|---|
| | Dietzel[a] 1173 K | Goleus[d] 1173 K | Lyon[a,c] 1473 K | Kucuk[c] 1673 K |
| Labware | 299 | 240 | 289 | 248 |
| E-glass | 386 | 343 | 378 | 373 |
| CRT panel | 310[b] | 286 | 290[b] | 290 |
| SLS | 319 | 297 | 306 | 305 |

a) $B_2O_3$ is not included in the calculation.
b) Additive coefficient of BaO is used for SrO.
c) $ZrO_2$ and ZnO are not included in the calculation.
d) $Fe_2O_3$ and $ZrO_2$ are not included in the calculation.

There are few data available describing the effect of surface tension on oxide melts. Experimental data on calcium-silicate foams at steady-state condition show that foam life (porosity) improves with increasing $P_2O_5$ content [86,87]. The $P_2O_5$ can be treated as a surface active specie, since they adsorb on the melt surface and decrease the surface tension of melts with various $CaO/SiO_2$ compositions [86].

According to Frenkel and Mackenzie model [88-90], viscous sintering of glass accelerates when surface tension increases. The density trend of E-glass (**Fig. 4.4**) could be affected by the lower surface tension which slows down the sintering and the $CaCO_3$ decomposes due to thermal instability before the E-glass forms a closed body. The XRD pattern shows crystallisation occurs in the range of $10^7$–$10^4$ Pa s. Solid inclusion [91] and crystallisation [92] decelerates the densification rate and can prevent fully densification. Hence, the anorthite, quartz and wollastonite formation could prevent sintering. The crystallisation also changes melt viscosity and the sintering kinetic, and, as discussed in **Sec. 3**, solid can destabilise a foam by changing drainage mechanism of foam films and by reducing the critical thickness of rupture [66,67].

The following serves as an example of a possible crystallisation effect on foaming ability. CRT panel glass and the SLS glass have similar surface tension (**Table 4.4**) and only a 2K difference of isokom temperature at $10^7$ Pa s (**Table 4.1**). At his viscosity value, the SLS glass reaches a density of 0.69±0.07 g/cm$^3$ and in comparison the CRT panel glass reaches 1.5±0.4 g/cm$^3$. Hence, the SLS glass has a greater ability to foam at this temperature (**Fig. 4.4a**). However, SLS glass crystallise mainly quartz at $10^7$ Pa s (**Fig. 4.3d**). Depletion of $SiO_2$ from glass melt decreases the viscosity and the SLS melt can expand faster. At lower viscosity ($10^4$–$10^6$ Pa s) the quartz crystallisation CRT panel glass expands more compare to SLS glass. The quartz crystallisation in SLS glass (up to 8 wt%) could be destabilising the foam at higher temperatures, causing a higher density.

Pokorny et al [46] finds a maximum expansion at 1073 K and 1173 K when soda-lime-silica glass is foamed with dolomite. The temperatures correspond to $\eta_g$ of $10^{5.5}$ Pa s and $10^{4.2}$ Pa s [93], respectively. They used a very low heating rate (0.8-2.5 K/min), which could promote excessive dolomite consumption. However; the results are still in good agreement with results obtained from the isokom foaming approach.

## 4.2 Percolation limit

In foam science, image analysis is an important tool for optimising foam stability (life time), foam capacity (maximum amount of gas the liquid can take up) or foaming ability (minimum conditions). Few attempts have been made to systematically study the foaming ability of glass melts at high viscosity range ($10^3$-$10^{12}$ Pa s). Bayer and Köse [16,17] used heating microscope to qualitatively evaluate the influence of concentration and particle size of SiC on the foaming ability of bottle glass. Attila et al. [94] measured the foaming ability of float glass using a displacement transducer to determine foaming onset and maximum expansion.

In many cases, foam glass with low density and closed pores is desired. The heating microscope provides directly the expansion behaviour of the glass melt and the corresponding density. The lowest density, however, is accompanied by a high degree of open pores. In the following, we discuss the use of heating microscope to define the heating range of foam glass with closed pores.

### Method

In collaboration with Hesse Instruments (Germany) we designed a heating microscope for monitoring the foaming process. Conventional heating microscopes can only employ small samples (normally 3x3x3 mm)

and the foams would only consist of very few bubbles. Our custom designed heating microscope can employ large samples which can foam up to 30 mm in diameter. The heating microscope records the silhouette area of illuminated samples as a function of temperature and time. A typical example is shown in (**Fig. 4.4**).

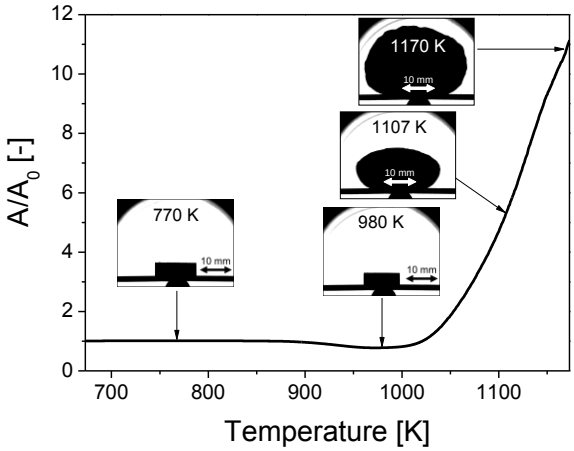


**Fig. 4.4** – Deformation curve: The pictures show the silhouettes of CRT panel glass being foamed with 7 wt% $MnO_2$ during heat-treatment at 10 K/min. The silhouettes area ($A$) is normalised to the area ($A_0$) at 423 K.

**Temperature profile in the heating microscope**

The heating microscope consists of a tube furnace. The thermocouple is located in an $Al_2O_3$ pipe underneath the sample. The $Al_2O_3$ can insulate the thermocouple and the recorded temperature will lag behind the actual temperature in the sample. We use several high purity standard materials to quantify the thermal lag (**Table 4.5**). The melting or decomposition temperatures of these materials are used as reference temperature. Changes in the area curves are attributed to the melting or decomposition temperature. The $T_{meas}$ agrees well with $T_{ref}$ (**Fig 4.5**). The $T_{meas}$ of Au, $BaCO_3$ and Al agrees very well with $T_{ref}$, whereas Ag deviates considerably.

**Table 4.5** – Chemicals used for temperature calibration of heating microscope. The melting- or decomposition temperature ($T_{ref}$) is measured as a sudden change in silhouette area. "Wire" refers to pieces (length ~9-11 mm). Strings (length ~20-50 mm) were bended and collapsed when melted.

| Chemical | Purity / company | Shape | $T_{ref}$ [K] |
|---|---|---|---|
| Zn | 99.999%, Aldrich | Wire (Ø 1 mm) | 693 |
| Al | 99.999%, Aldrich | Wire (Ø 1 mm) | 933 |
| $BaCO_3$ | 99.999%, Aldrich | Pressed powder | 1083 |
| Ag | 99.99%, Aldrich | String + wire (Ø 0.5 mm) | 1235 |
| Au | 99.99%, Aldrich | String (Ø 0.5 mm) | 1337 |

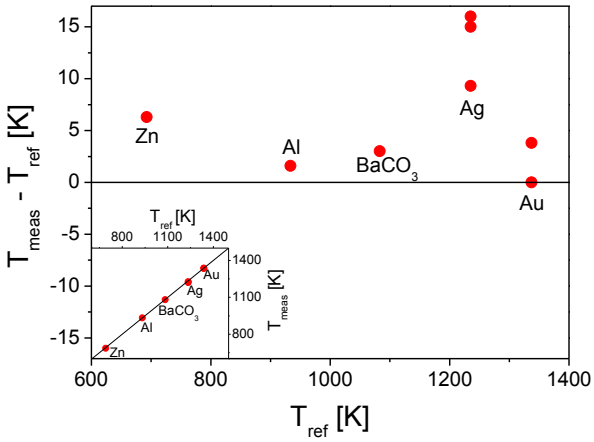


**Fig. 4.5** – Measured temperature ($T_{meas}$) compared with the reference melting or decomposition temperature ($T_{ref}$). The inset shows the measurement error. The standard deviation of $BaCO_3$ originates from the difficulty of finding a characteristic area change attributed to the decomposition.

A furnace has commonly a thermal gradient between the interior sides and the sample position. The heating microscope is not an exception. The thermal gradient is determined by placing Al pieces at different radial positions on the alumina plate. The area change of each Al piece is attributed to the melting of Al. When comparing the temperature at 15 mm away from the centre (Position = 0 mm), the temperature can diverge up to 14 K when heating at 5 K/min (**Fig. 4.6**). When heating at 30 K/min, the temperature diverges 28 K. It is important to have this in mind, since foam glass expands during heating and will therefore be exposed to different heating intensity throughout the sample.

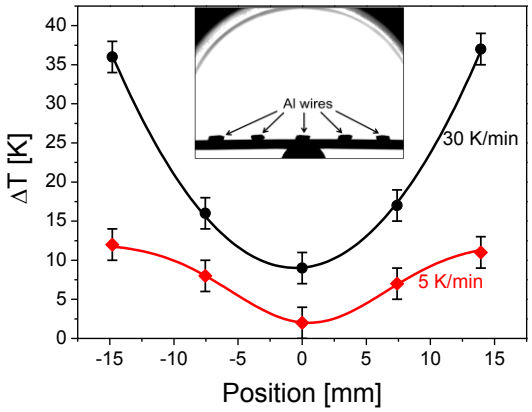


**Fig. 4.6** – Temperature distribution at 933 K in axial position at different heating rates (see legend). $\Delta T = T_{meas} - T_{ref}$, where $T_{meas}$ is the recorded temperature at which the area change begins and $T_{ref}$ is the melting temperature of Al ($T_{ref}$ = 933 K). The alumina sheath around the thermocouple is located underneath the sample (see the bottom side of inset picture). The lines are guides for the eye.

**Characteristic temperatures and repeatability**

From the sample area curve ($A/A_0$) and the derived curve ($r_A = d(A/A_0)/dt$), several characteristic temperatures will be defined in the following (**Fig. 4.7**). The onset of sintering ($T_s$) is per definition the temperature at which $A/A_0$ = 0.95. Foaming temperature ($T_f$) is defined as the minimum area of the sample before foaming occurs ($r_A$ = 0). The onset of foaming ($T_{f,onset}$) is defined as the intersection point of the tangents at which the glass is sintered and when expansion occurs. The temperature of maximum expansion rate ($T_{r,max}$) occurs when $r_A$ reaches a maximum. Each characteristic temperature can be determined within ±4 K (**Table 4.6**).

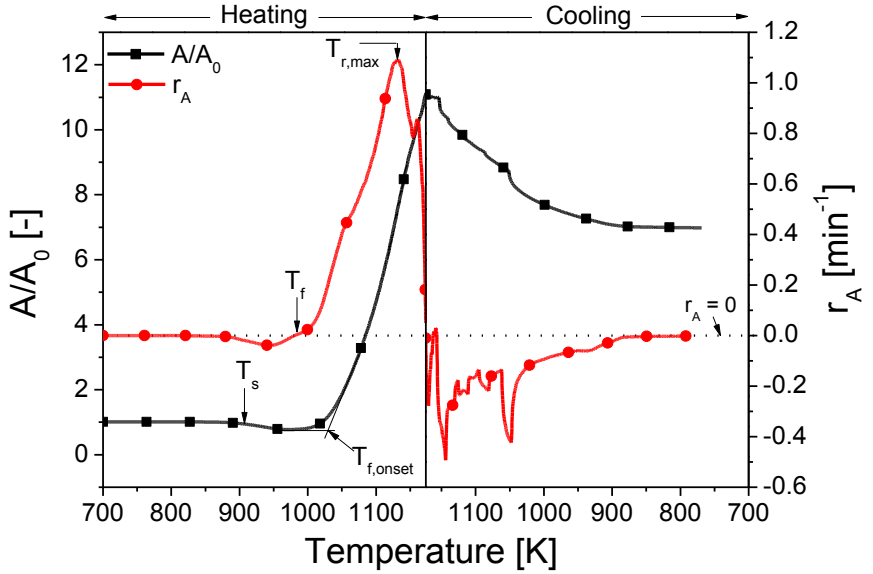


**Fig. 4.7 –** Deformation curve: Characteristic temperatures for foaming of glass melt. $A/A_0$ is the normalised silhouettes area and $r_A$ is the derivative, $d(A/A_0)/dt$. The characteristic temperatures are defined in the text. Heating rate is 10 K/min.

**Table 4.6** – Sintering temperature ($T_s$) and foaming temperature ($T_f$) of five repeating measurements. $T_s$ is defined as the 5% area shrinkage ($A/A_0 = 0.95$) and $T_f$ is defined at $r_A = 0$ when $T > T_s$. Heating- and cooling rate is 10 K/min.

| Run # | $T_s$ [K] | $T_f$ [K] | $T_{f,onset}$ [K] | $T_{r,max}$ [K] |
|---|---|---|---|---|
| 1 | 906 | 977 | 1034 | 1128 |
| 2 | 903 | 971 | 1032 | 1133 |
| 3 | 906 | 975 | 1034 | 1128 |
| 4 | 903 | 972 | 1032 | 1126 |
| 5 | 905 | 972 | 1031 | 1129 |
| Average | 905 ± 2 | 973 ± 4 | 1033 ± 2 | 1129 ± 4 |

The heat-treatment of glass powder and foaming agent results in sintering and subsequent expansion. After reaching maximum temperature (1173 K) the foam glass cools to room temperature. During cooling distinct drops in the $A/A_0$ curve appears (**Fig. 4.7**). These are related to bursting of very large bubbles at the sample surface.

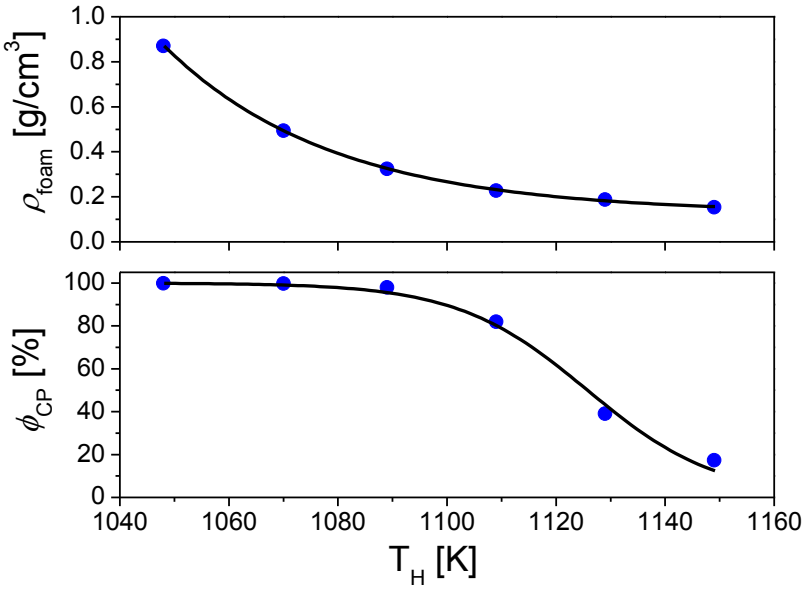


**Fig. 4.8 –** Foam density ($\rho_{foam}$) and closed porosity ($\varphi_{CP}$) of foam glasses obtained by heating in a heating microscope to temperature ($T_H$) at 10 K/min and subsequently cooling the foam glass with ~20-30 K/min to the glass transition temperature (803 K). The $\rho_{foam}$ is fitted to an exponential decay function whereas the $\varphi_{CP}$ data are fitted to a Boltzmann sigmoidal function **Eq.** (**4.2**).

**Expansion rate and percolation limit**

The expansion rate ($r_A$ [min$^{-1}$]) reaches a sharp maximum at $T_{r,max}$. Before $T_{r,max}$ is reached, the pores remains closed. As the temperature increases, the bubble pressure increase and the viscosity decreases. This accelerates cell wall thinning and, hence, coalescence rate. At $T_{r,max}$ the foam has become percolated and the escapes out of the sample. The foam expansion occurring above $T_{r,max}$ is controlled by the bubble growth of the remaining closed pores. To show how $T_{r,max}$ is linked to the closed porosity several samples were foamed in the heating microscope up to different temperatures ($T_H$) and then subsequently cooled fast to $T_g$. The foam density ($\rho_{foam}$) and closed porosity ($\varphi_{CP}$) decreases as $T_H$ is increased (**Fig. 4.8**). The $\varphi_{CP}$ data are fitted with a Boltzmann sigmoidal function:

$$\varphi_{cp}(T_H) = \frac{\varphi_{cp,1} - \varphi_{cp,0}}{1 + e^{(T_H - T_{50})/dT}} + \varphi_{cp,0} \qquad \textbf{(4.2a)}$$

where $T_H$ is the treatment temperature, $T_{50}$ is the centre value, i.e. $\varphi_{CP}(T_{50})$ = 50% and $dT$ is the temperature step. The asymptotic values are treated as

constants. At low temperatures the sintered body has 100% closed pores, i.e. $\varphi_{CP,1}$ = 100%. Increasing the temperature the pores become open. If we assume the temperature increase only induce coalescence and ignore bubble nucleation and foam collapse, we can set $\varphi_{CP,0}$ = 0%. $T_{50}$ and $dT$ are fitting values. We can simplify the function to:

$$\varphi_{\mathrm{cp}}(T_H) = \frac{1}{1+e^{(T_H - T_{50})/dT}} \qquad \textbf{(4.2b)}$$

A fitting gives a $T_{50}$ of 1125.8±1.3 K. In comparison, $T_{r,max}$ is 1129±4 K. $T_{50}$ is expected to be lower than $T_{r,max}$, since coalescence proceeds during cooling and $T_{r,max}$ is an *in situ* value. However, both values agree with each other within the error limit, indicating that the maximum expansion rate is reached at $T_{r,max}$ when the closed porosity is 50%.

**Applying the percolation limit**

Köse [17] suggested that the foaming should be stopped before maximum foam expansion is reached, which occurs at higher temperature than $T_{r,max}$. Here, I narrow down the temperature regime of foaming, by defining the optimal temperature for forming foam glass with closed pores to be in the range of:

$$T_{f,onst} < T < T_{r,max} \qquad \textbf{(4.3)}$$

Heating microscope can be used to effectively determine optimum conditions for forming foam glass with closed pores. Köse [16,17] investigated with heating microscope the influence of SiC concentration on the foaming ability of bottle glass (**Fig. 4.8**). The results clearly indicate the expansion ability of bottle glass melt. However, the results do not directly show if the foams become percolated.

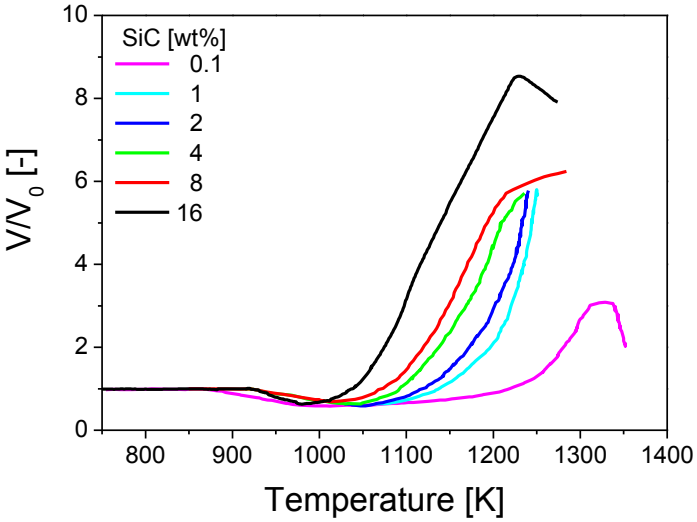


**Fig. 4.8** – Deformation curve of bottle glass foamed with different concentrations of SiC (see legend). The data originate from [16]. The heating rate was 12 K/min [17]. $V$ is the volume of the foam and $V_0$ is the volume at room temperature.

We can use the same procedure as described above to extract $T_f$, $T_{f,onset}$ and $T_{r,max}$ from the deformation curves in **Fig. 4.8**. The results are shown in **Fig. 4.9**. $T_f$ increases from 0.1 wt% to 1 wt%, but drops again with increasing SiC concentration. $T_{r,max}$ and $T_{f,onset}$ continuously decreases with SiC concentration. Comparing **Fig. 4.8** and **4.9** shows the sensibility of using $T_{f,onset}$ instead of $T_f$ to determine the temperature regime of foaming. If the glass melt is sintered to a densified body in wide temperature range the $T_f$ temperature cannot represent the start of foaming. Hence, $T_{f,onset}$ is a better descriptive parameter for the beginning of foaming.

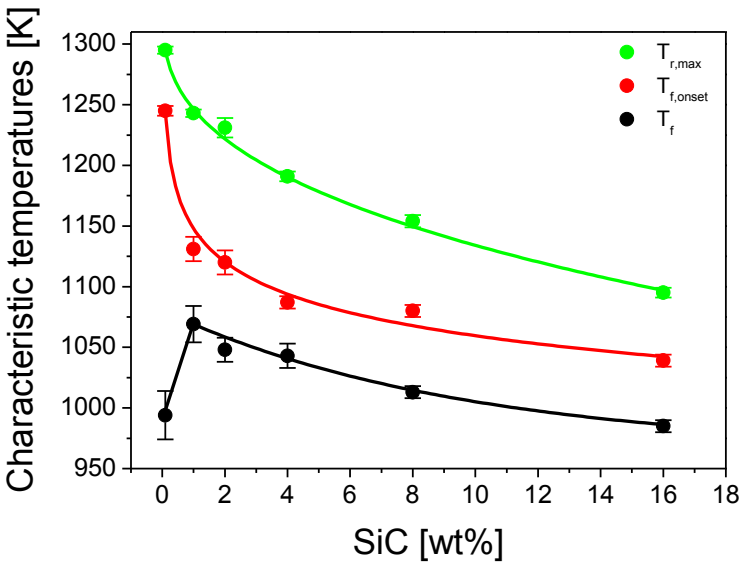


**Fig. 4.9 –** The foaming temperature ($T_f$), foaming onset temperature ($T_{f,onset}$) and temperature of maximum expansion rate ($T_{r,max}$). The characteristic temperatures are determined from Fig. 5.8. The lowest SiC concentration is 0.1 wt%. The lines are guides for the eye.

Heat-treatment at $T_{f,onst} < T < T_{r,max}$ produces foam glass with closed pores. For thermal insulation applications, the foam glass with lowest density (or maximum expansion) and closed pores is preferred. To reach the maximum expansion within $T_{f,onst} < T < T_{r,max}$, the temperature should reach close to $T_{r,max}$. If temperature reaches $T_{r,max}$, the foam is already percolated. However, to be able to extract data representing foam glass with closed pores and the lowest density, we simplify by assuming that any heat-treatment to $T_{r,max}$ will result in foam glass with closed pores. Using this approximation we can extract the foam expansion values ($V/V_{0,max}$) at $T_{r,max}$ from **Fig. 4.8**. The results show a maximum in foam expansion occurs when 2 wt% SiC (**Fig. 4.10**). Using higher SiC concentration improves expansion, but result in highly percolated foams. SiC concentrations below 1 wt% do not allow efficient foam expansion under dynamic heat conditions, since the temperature becomes too high before a large foam volume is reached and the foam will instead start to coalescence very fast and eventually collapse due to the low viscosity.

My studies show that the optimal foaming can be tuned within the SiC concentration of 1 wt% < [SiC] < 4wt%. TECHNOpor uses flat-, bottle and

lamp glass with < 2wt% SiC in their foam glass production [95]. Hence, the findings agree well with industrial conditions.

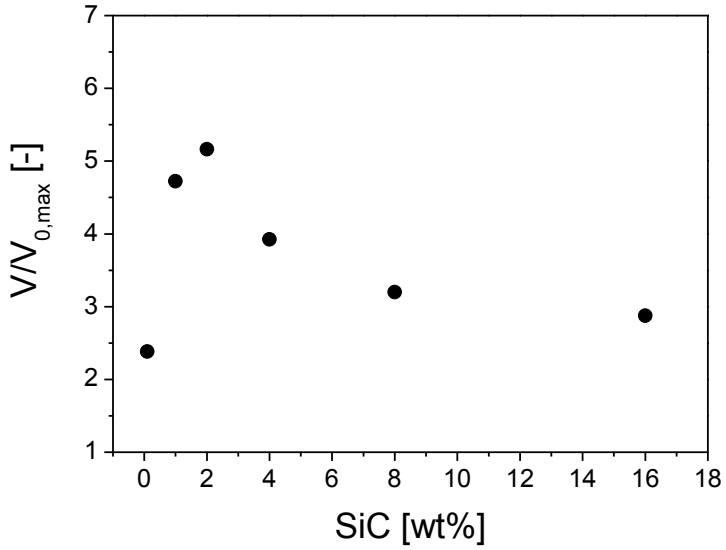


**Fig. 4.10 –** Normalised foam volume ($V/V_{0,max}$) at the temperature of maximum expansion rate ($T_{r,max}$).

### 4.3 Summary

Knowing approximately the optimal condition for foaming accelerates time consuming development of new recipes. The methods discussed here were based on glass melt viscosity and several characteristic temperatures derived from deformation curves and were discussed according to foam capacity and percolation limit. It was experimentally shown that foam density is lowest in a viscosity regime of $10^4$-$10^6$ Pa s. This is also in accordance with **Fig. 3.2** where a minimum in foam density is found between $10^{4.5}$-$10^6$ Pa s for most $Na_2CO_3$ concentrations. Heating microscope is a powerful tool to assess the temperature regime for foaming of glass melt. In general, the glass melt should be foamed in the temperature regime of $T_{f,onset} < T < T_{r,max}$. For CRT panel glass, this is 1033 K < $T$ < 1129 K or in viscosity values: $10^{5.9}$ Pa s < $\eta_g$ < $10^{4.6}$ Pa s. These values are also in accordance with the findings found with the isokom foaming approach and in accordance with Pokorny et al [46]. The viscosity results are summarised in **Table 4.7**.

**Table 4.7** – Summary of results. $\eta_g$ is the viscosity of bubble- and crystal free glass melt. SLS refers to soda-lime-silica glass. Isokom refers to the results of **Sec. 4.1**. HSM refers to heating microscope results, **Sec. 4.2**.

| Method | Glass | Foaming agent | $\eta_g$ [Pa s] | Ref |
|---|---|---|---|---|
| Isokom | Labware | 2wt% $CaCO_3$ | $10^4$-$10^6$ | This work |
| Isokom | E-glass | 2wt% $CaCO_3$ | $<10^4$ | This work |
| Isokom | CRT panel | 2wt% $CaCO_3$ | $10^4$-$10^6$ | This work |
| Isokom | SLS | 2wt% $CaCO_3$ | $10^6$-$10^{5.5}$ | This work |
| Dynamic | CRT Panel | 6-22wt% $Na_2CO_3$ | $10^{4.5}$-$10^{6.0}$ | Paper I |
| HSM | CRT panel | 7wt% $MnO_2$ | $10^{4.6}$-$10^{5.9}$ | This work |
| HSM | Bottle | 2 wt% SiC | $10^{3.7}$-$10^{4.9}$ | This work |
| Dynamic | SLS | 3 and 5wt% Dolomite | $10^{4.2}$-$10^{5.5}$ | Based on [46] |

# 5. Thermal Conductivity

Many foam glass studies report thermal conductivity for a range of densities. In general, the thermal conductivity decreases linearly with density [PaperI, 15,18,24,94,96-98]. Comparing one data set with another is very difficult and often impossible, because basic information is lacking, e.g. temperature at which thermal conductivity is measured. In addition, not everyone reports the chemical composition of the gas and solid matrix, the degree of closed porosity and crystallinity of solid matrix. A comparison is therefore in many cases futile.

The thermal conductivity of foam glasses from my studies were measured in a climate chamber with an Isomet surface probe (2401, Applied Precision). Samples had a diameter of 6 cm and height of ~4-6 cm.
The cell pressure of several foam glasses was measured by first crushing the sample in a gas-tight crushing cell. The pressure inside the cell was measured by inserting a syringe through a rubber stopper and the pressure was calculated from the volume contraction of a syringe.

## 5.1 Heat Transfer Mechanism

### Gas conductance

The thermal conductivity of gas is a factor 50 lower compared to commercial float- and bottle glass, but account for 40-50% of the total thermal conductivity of foam glass. It is therefore important to control the gas atmosphere. In the sinter-foaming approach the gas atmosphere is controlled through the implementation of foaming agent. Low thermal conducting gasses such as krypton and $SO_2$ are not realistic since almost no compounds with krypton exist, and $SO_2$ is not used due to the health risks involved. $CO_2$ is already used in commercial foam glass today synthesised through oxidising carbonaceous substances. Carbonates like $CaCO_3$ and $Na_2CO_3$ would preferably be used to induce $CO_2$ entrapment. However, as discussed in chapter 2, it is difficult to produce foam glass with low density and foam structure with closed pores.

### Solid conductance

The mechanism controlling the thermal conductivity of glasses is not well understood and the data available are scarce [99]. This is probably due to the difficulties of obtaining reliable data. The thermal conductivity of common post-consumer glass is calculated based on their composition (**table 5.1)**. The calculations are on Choudhary and Potter's [100] linear statistical

model. The thermal conductivity of CRT panel glass is 11-12% lower than the common float and bottle glass composition. This is advantageous for thermal insulation applications.

**Table 5.1 –** Thermal conductivity of gasses and glasses at 298 K. The solid conductivity ($\lambda_s$) of glasses is calculated from a linear model based on the chemical composition [100].

| Gas type | $\lambda_g$ [mW $m^{-1}$ $K^{-1}$] |
|---|---|
| Air | 26 |
| $O_2$ | 26 |
| CO | 25 |
| $CO_2$ | 18 |
| $H_2O$ | 17 |
| Ar | 17 |
| Kr | 8 |
| $SO_2$ | 8 |

| Glass type | $\lambda_s$ [mW $m^{-1}$ $K^{-1}$] |
|---|---|
| Float | 1073 |
| Bottle | 1083 |
| CRT panel | 950 |

The solid matrix of foam glass is altered when foaming agent slowly dissolves into the glass melt. This will also affect the thermal conductivity. Since the foaming agent is inhomogeneously incorporated into the glass matrix, several paths for the thermal transport may exist. The foaming agent is a crystalline material and it can serve as nucleation agent and induce crystallisation. Crystalline materials [101,102] are often more conducting than the amorphous silicate glasses [103]. It is therefore preferably to allow the foaming agent to dissolve in the glass melt and avoid crystallisation. On the other hand, interfacial resistance between solid inclusions and glass matrix can scatter the phonons [104-106], leading to a lower thermal conductivity of the solid part. As shown in **Fig. 2.10** and **Fig. 3.2**, $Mn_2O_3$ and Si-rich inclusions are integrated in the glass matrix. Nevertheless, they take up a minor part of the solid volume as indicated by the SEM (**Fig. 2.9** and **Fig. 3.2**) and XRD results (**Fig. 2.9**), thus only few boundaries exist. Hence, the phonon scattering due to grain boundaries will not significantly influence the thermal conductivity. Therefore, only the solid and gas conduction needs to be defined when predicting the thermal conductivity of foam glass.

**Radiation and convection**

Radiative heat transfer is probably the most complex heat transfer to quantify. It depends on porosity, size and geometry of pores, thickness of cell wall and struts and the composition of gas and solid matrix. Infrared, UV and visible light contributes to the radiative heat transfer [107]. Infrared influences significantly the overall thermal conductivity of highly porous materials [108]. This is often seen for organic foams, such as expanded polystyrene [109], polyurethane [109] and aerogels [110]. It declines with decreasing porosity [109] and becomes insignificant when $\varphi$ < 94% for organic foams. The thermal radiation is not quantified in this study. In addition, silicate glasses are almost completely opaque for mid- and near infrared radiation and our foam glasses have very low transmittance for the visible light.

Convective heat-transfer of gas occurs due to forced movement of the gas (e.g. windy conditions) or due to thermal induced convection. The foam glasses studied here have both high degree of open- and closed porosity. However, the thermal conductivity measurements are performed in still air, which did not allow forced convection to occur. Thermal induced convective heat-transfer is not significant for porous material with high density and small pores. Skochdopole [111] shows that for air filled polystyrene (25.3 kg/m$^3$) convective heat-transfer becomes important when pore size is above 4 mm. Besides, since my samples are measured by placing the detector on the top surface, thermal induced convective heat transfer is not measured.

When pores are small (< 10 μm) [110,112], the thermal conductivity of the gas phase is reduced (known as the Knudsen's effect). Decreasing the pressure inside the pores reduces the thermal conductivity even further [110,113]. The pressure in foam glass is within 0.3–0.8 atm. Our foam glasses have only few pores smaller than 10 μm. Therefore, the combined effect of the decreased pressure reduction and small pores should be insignificant for the foam glasses in this study.

Open pores permits foam gas ($O_2$) to exchanges with the surrounding atmosphere (air) and convective heat transfer to contribute to the thermal conductivity. The thermal conductivities of $O_2$ and air are similar around 283 K; hence, the degree of closed porosity, in terms of different gas composition, does not influence the overall thermal conductivity. The modelling results of Köse and Bayer [17,25] suggests that pore size (diameter = 1–5 mm) strongly influences the thermal conductivity of foam glass ($\rho_{foam}$ = 0.2–0.4 g/cm$^3$). By comparing foam density (**Fig. 3.1**) and pore size (**Fig. 3.2**) with the overall thermal conductivity ($\lambda_f$) of our foam glasses (**Fig. 5.1**), we find that the pore size has no measurable effect on the thermal conductivity of foam glass with densities between 0.2–0.4 g/cm$^3$ ($\varphi$ = 86–

92%). Wu *et al.* [15] reported the similar observation for their glass-ceramic foams ($\varphi$ = 85–94%).

**Thermal Conductance Models**

Since convective and radiative heat transfer is not significant factors in the heat transfer, they are not considered in the follow presentation of thermal conductivity models. Conduction through the solid and gas is treated as decoupled mechanisms. Only under special conditions must this assumption be modified. A few studies predict the thermal conductivity of foam glass using analytical [15] and numerical models [15,17,96]. Porous materials can ideally be considered as cubic gas cells arrangement periodically in a solid matrix [114]:

$$\lambda_f = \frac{\lambda_s[\lambda_s+\varphi^{2/3}(\lambda_g-\lambda_s)]}{\lambda_s+(\lambda_g-\lambda_s)(\varphi^{2/3}-\varphi)} \quad \textbf{(5.1)}$$

where $\lambda_s$ is the solid conductivity, $\lambda_g$ is gas conductivity and $\lambda_f$ is the conductivity of the foam.

Landuaer [115] developed a percolation model of two mediums dispersed randomly in each other. The Landauer model predicts very well the thermal conductivity of porous zirconia ($\varphi$ = 44–73%) [112]:

$$\lambda_f = \frac{1}{4}\Big[\Big(\lambda_g(3\varphi-1)\Big) + \lambda_s(3\varphi_s-1) + \Big(\big[\lambda_g(3\varphi-1)+\lambda_s(3\varphi_s-1)\big]^2 + 8\lambda_s\lambda_g\Big)^{1/2}\Big] \quad \textbf{(5.2)}$$

where $\varphi_s$ is solidisity ($1-\varphi$). Schuetz and Glicksman [116] derived a simple linear model from porous materials with cubic cells (Eq. 6.3 and 6.4):

$$\lambda_f = \lambda_g + K(1-\varphi)\lambda_s \quad \textbf{(5.3)}$$

$$K = \tau\left(\frac{2}{3} - \frac{f_s}{3}\right) \quad \textbf{(5.4)}$$

where $f_s$ denotes the amount of the solid located in the strut. $f_s$ = 0 when the entire solid is located in pore wall and $f_s$ = 1 when all the solid resides in the strut. The factor ($2/3 - f_s/3$) represents the amount of the solid aligned parallel to the heat flow. The $\tau$ is a tortuosity factor. Schuetz and Glicksman showed for staggered cubic cells, that the solid conduction can reduce up to 20% ($\tau$ = 0.8) due to the tortuous path of heat transfer through the solid matrix [116,117]. Solórzano *et al.* [118] shows similar with finite element

calculations that the solid tortuosity influences the thermal conductivity of cellular materials. However, so far there has been no experimental verification of the tortuous effect on thermal conductivity. **Eq. 5.3** and **5.4** can be used to estimate the lower limit of the thermal conductivity of a foam glass by assuming all solid resides in the struts ($f_s$ = 1) and the conduction through the solid is very tortuous ($\tau$ = 0.8). An upper limit calculation of Schuetz-Glicksman model ($f_s$ = 0, $\tau$ = 1) result in a similar trend as the Russell model for $\rho_{foam} < 0.5$ g/cm$^3$.

### 5.2 Foam Glass with $O_2$/air

Foam glasses with open pores will have foam gas exchange with air. Therefore, the gas composition can vary within the sample. Foam glass foamed with $MnO_2$ can serve to prepare foam glass with ideal gas composition. Since the gas conduction of $O_2$ and air is very similar (**Table 6.1**), the gas conduction should not be influenced if the pores are open or not. Hence, $\lambda_g$ is regarded constant regardless of degree of closed porosity. The conductivity of the solid matrix is a complex function of CRT panel glass wherein manganese oxide is dissolved inhomogeneously and crystalline $Mn_2O_3$ (**Fig. 2.9**). The solid matrix consist of 93wt% (~96vol%) CRT panel glass and can be treated ideally as one phase consisting of CRT panel glass. The $\lambda_s$ of CRT panel is calculated using the statistical linear model [100] (**Table 5.1**). The $\lambda_s$ value is temperature corrected, since the foam glasses are measured at ~283 K. The thermal conductivity of many silicate glasses [119,120] decreases on average 2.7 % when the temperature drops from 298 to 283 K. Hence, a temperature corrected value of $\lambda_s$ = 0.925 W m$^{-1}$ K$^{-1}$ is used to calculate the thermal conductivity of foams. The models are calculated at 283 K using $\lambda_g$ = 0.025 W m$^{-1}$ K$^{-1}$ for air/$O_2$ atmosphere.

The experimental data together with the models are presented in **Fig. 5.1**. The data follows in linear trend. At the lower densities the data deviates from the linear trend. The Russell model overestimates the experimental data and the Landauer model underestimates the data. The lower limit model of Schuetz-Glicksman predicts slightly lower thermal conductivity than the experimental data (**Fig. 5.1**). The SEM images show that cell walls are present. Therefore we can assume $f_s < 1$. The $f_s$ value is obtained from many organic foams by measuring mean pore wall thickness, average pore diameter and strut diameter under ideal pore geometry [108,121,122]. However, such detailed structural information is not available for the foam glass. If we instead assume $K$ = 0.34 the model shows a good agreement between model and experimental data (**Fig. 6.1**).

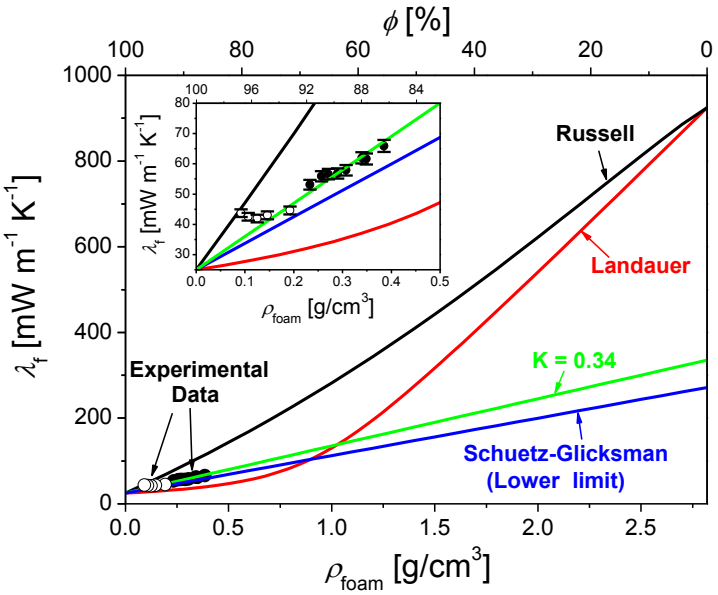


**Fig. 5.1** – The thermal conductivity ($\lambda_f$) of foam glasses prepared with $MnO_2$. $\rho_{foam}$ is the foam density and $\varphi$ is the porosity. The inset zooms in on the experimental data. The error bars represent 3% of experimental $\lambda_f$ values. The data are obtained at 283.7±0.6 K. The models are calculated or fitted using $\lambda_s$ = 0.925 W m$^{-1}$ K$^{-1}$ (CRT panel glass) and $\lambda_g$ = 0.025 W m$^{-1}$ K$^{-1}$ (air/$O_2$). The data are from ● [Paper I] and ○ this work.

Deviations from the linear model are observed at the lowest densities. The pores are large and open. Hence, increase contribution from radiative heat transfer can be expected.

König et al. [18,123] measured thermal conductivity on CRT panel glass foamed with $MnO_2$ and carbon. Such mixture could potentially result in $CO_2$ filled foam glass. However, the decomposition of $MnO_2$ to $Mn_3O_4$ releases pure $O_2$, inducing the burn-out of carbon before the glass melt sinters a closed structure. In addition, the samples had a high degree of open porosity [18,123] and majority of the gas would therefore consist of air. The data of König et al. [18,123] are shown in **Fig. 5.2** together with foam glasses formed with $MnO_2$. The data agrees well with $O_2$/air filled foam glass and follows the linear trend well. Small amount of C could remain in the samples after densification. Majority of carbon would be converted to CO [124]. The conductivity of CO is comparable to air (**Table 5.1**) and the CO effect should not be measurable. The closed porosity is not reported for these data, but the high density foam glasses (0.17-0.18 g/cm$^3$) should contain a larger degree of closed pores [18].

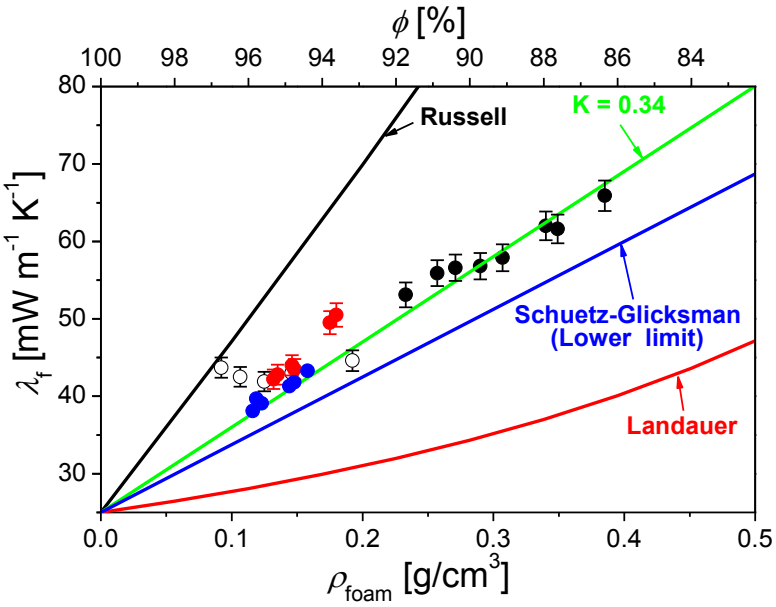


**Fig. 5.2 –** The thermal conductivity ($\lambda_f$) of foam glasses prepared with $MnO_2$. $\rho_{foam}$ is the foam density and $\varphi$ is the porosity. The inset zooms in on the experimental data. The error bars represent 3% of experimental $\lambda_f$ values. The data are obtained at 283.7±0.6 K. The models are calculated or fitted using $\lambda_s$ = 0.925 W m$^{-1}$ K$^{-1}$ (CRT panel glass) and $\lambda_g$ = 0.025 W m$^{-1}$ K$^{-1}$ (air/$O_2$). The data are from ● [Paper I], ○ this work, König et al. [123] and ● König et al. [18].

**Table 5.2 -** Foam density ($\rho_{foam}$), porosity ($\varphi$), thermal conductivity ($\lambda_f$) and closed porosity ($\varphi_{CP}$) of foam glass prepared with CRT panel glass and $CaCO_3$. $\lambda_f$ is measured at 283 K. The $\varphi_{CP}$ data from König et al. [24] are recalculated with **Eq. (2.2)** using $\rho_s$ of 2.74 g cm$^{-3}$.

| $\rho_{foam}$ [g cm$^{-3}$] | $CaCO_3$ [wt%] | $\varphi$ [%] | $\lambda_f$ [mW m$^{-1}$ K$^{-1}$] | $\varphi_{CP}$ [%] | Ref |
|---|---|---|---|---|---|
| 0.240 | 4 | 91.2 | 50.2 | 72.8 | [24] |
| 0.242 | 4 | 91.2 | 53.1 | 83.6 | [24] |
| 0.267 | 4 | 90.2 | 51.3 | 63.6 | [24] |
| 0.223 | 2 | 92.1 | 52.0 | 7.0 | This work |
| 0.312 | 2 | 88.9 | 58.9 | 62.5 | This work |
| 0.355 | 2 | 87.4 | 62.8 | 76.3 | This work |
| 0.370 | 2 | 86.9 | 64.5 | 76.2 | This work |
| 0.433 | 2 | 84.6 | 69.0 | 89.8 | This work |

### 5.3 Foam Glass with $CO_2$/air

To induce $CO_2$ filled foam glass, $CaCO_3$ is used as foaming agent. The resulting data are shown in **Table 5.2** Due to the difficulties of foaming with $CaCO_3$, foam glass with 100% closed pores are not obtained. All of them except one have a closed porosity between 62.5-89.8 %. The data follows a linear trend (**Fig. 5.3**) and follows the linear air/$O_2$ model. This is surprising; since the presence of $CO_2$ should lower the overall thermal conductivity by ~9 mW/(mK). A small amount of Fe is present in the glass powder mixture from the crushing procedure. The $CO_2$ could oxidise the Fe. In addition, metal oxides presence in multiple valence states could also become oxidise. The reduction of $CO_2$ would lead to CO enriched gas composition in the pores and an increase of thermal conductivity (**Table 5.1**). The amount of Fe and metal oxides which can be oxidised, however, is very small. Hence, only a small contribution from CO is expected.

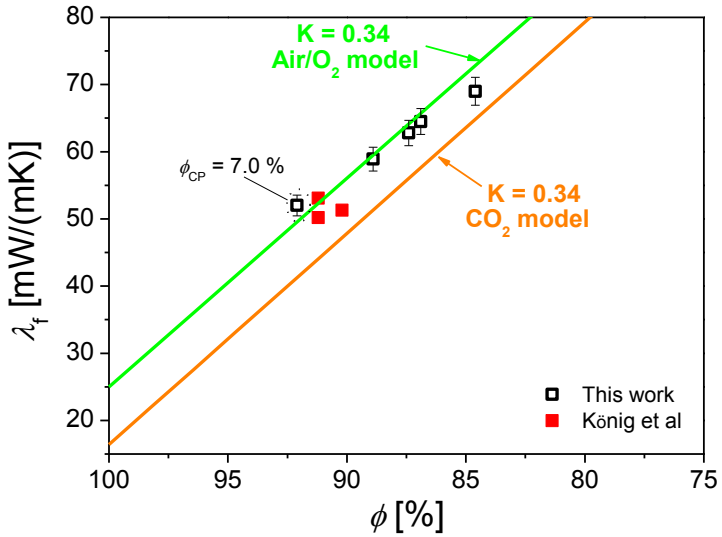


**Fig. 5.3 –** The thermal conductivity ($\lambda_f$) of foam glasses prepared with $CaCO_3$. $\rho_{foam}$ is the foam density. The error bars represent 3% of experimental $\lambda_f$ values. The data is obtained at 283 K. The models are calculated using $\lambda_s$ = 0.925 W $m^{-1}$ $K^{-1}$ (CRT panel glass) and $\lambda_g$ = 0.025 W $m^{-1}$ $K^{-1}$ (air/$O_2$) and $\lambda_g$ = = 0.016 W $m^{-1}$ $K^{-1}$ ($CO_2$). The models are calculated with Eq. (**5.3**) using $K$ = 0.34. The data are from □ this work and ■ König et al. [24].

**Fig. 5.4** compares the thermal conductivity data of all available data for foamed CRT panel glass. The thermal conductivity of foam glasses foamed with $CaCO_3$ does not differ significantly from foam glasses foamed with

$MnO_2$ and $MnO_2$/C. The addition of foaming agent alters thermal conductivity of the solid phase. The thermal conductivity mechanism of glass is fairly understood [99] and is therefore difficult to predict the impact of composition alterations. The additivity model of Choudhary and Potter [100] predicts manganese oxide has a negative impact on the thermal conductivity of glasses. The application limit of this model is not reported. Ghoneim et al [125] show for $BaO$-$B_2O_3$-$SiO_2$ glasses that addition of 0.1 or 0.99 wt% $MnO_2$ increases the thermal conductivity. Choudhary and Potter [100] summarised several additivity models. All the models had CaO as a positive additive factor for the thermal conductivity for a wide range of silicate glasses [80,126-129]. Hence, foaming with $CaCO_3$ could increase the solid conductivity and $MnO_2$ could decrease the solid conductivity of foam glass.

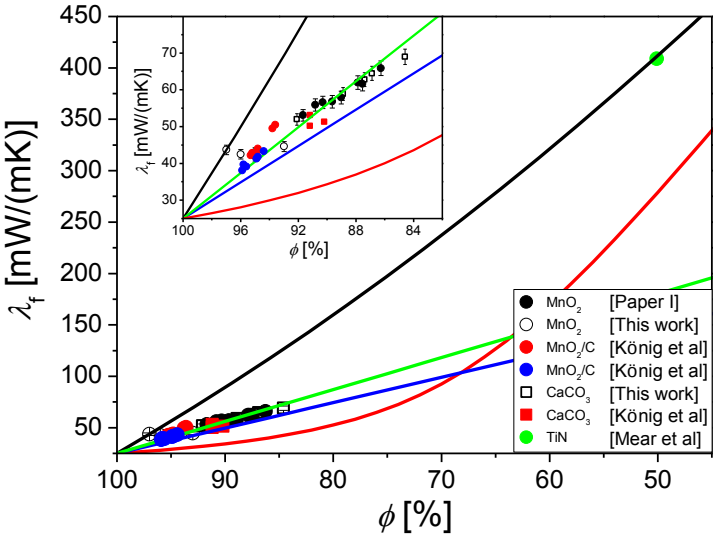


**Fig. 5.4** – The thermal conductivity ($\lambda_f$) of foam glasses prepared from CRT panel glass and with different foaming agents (see legend). $\rho_{foam}$ is the foam density. The error bars represent 3% of experimental $\lambda_f$ values. The data are obtained at 283 K. The models are calculated using $\lambda_s$ = 0.925 W m$^{-1}$ K$^{-1}$ (CRT panel glass) and $\lambda_g$ = 0.025 W m$^{-1}$ K$^{-1}$ (air/$O_2$). ─ Russell model, ─ Landauer model, ─ Schuetz-Glicksman lower limit model, ─ Linear model, $K$ = 0.34 **Eq. (5.3)**. ● [Paper I], ○ This work, ● König et al [18], ● König et al [123], □ This work, ■ König et al [24]. The data point from ● Mear et al [97,130] is temperature corrected from 298 K to 283 K with -4.8%. Foam density data from König et al [18,123] are calculated in porosity by assuming $\rho_s$ = 2.82 g/cm$^3$.

A data point for a high density foam glass prepared with TiN [97,130] is included in **Fig. 5.4**. When comparing this data with the low density range, it indicates that thermal conductivity of foam glasses will decrease sharply with increasing porosity within the porosity range of 65-85% (density range of ~0.5-1.3 g/cm$^3$). This indicates that a linear conductivity model applies down to the porosity of 80%. However, the thermal conductivity of glass-ceramic foams can exhibit a linear range in a much wider porosity range ($\varphi$ = 47-94%).

## 5.4 Summary

The thermal conductivity of foam glasses prepared from CRT panel glass were compared. Foaming agents such as $MnO_2$, $CaCO_3$, $MnO_2$/C and TiN were used to make the foam glasses. The impact of foaming agent was discussed. The use of $CaCO_3$ could possibly increase the solid conductivity, whereas $MnO_2$ could decrease it. The thermal conductivity of foam glasses foamed with $MnO_2$, $CaCO_3$, or $MnO_2$/C follows in general a linear trend with porosity.

# 6. General Discussion

**Foaming Mechanism**

$MnO_2$ is a suitable foaming agent for CRT panel glass, float glass and bottle glass, since it releases gas at the foaming regime. Manganese oxide can work as nucleation agent and induce crystallisation in float glass and bottle glass, but this can be prevented using crystallisation inhibitor [16,21]. CRT panel glass, on the other hand, has excellent glass stability. $MnO_2$ can be employed with additional agents (e.g. SiC, $Si_3N_4$). It is often assumed that $MnO_2$ causes the oxidation of SiC [22,50] or $Si_3N_4$ [49]. Since $MnO_2$ reduces to $Mn_2O_3$ between 860–990 K, it is more likely that the dissolution of $Mn_2O_3$ and subsequent reduction according to equilibrium **Eq. (2.4)** releases $O_2$ which oxidises SiC and $Si_3N_4$ if the glass melt itself is not an oxidising medium.

A useful strategy to gain lower foam density is to decrease particle size of glass cullet and foaming agent. This has shown to be useful with systems including foaming agents such as carbon [27], $MnO_2$ [18] or AlN [64] which involves gas forming redox reactions. However, when carbonates like $CaCO_3$ [24] or dolomite [46] are involved, the particle size must be optimised if foam glass with low density is needed. This phenomenon can be explained by the proposed reaction mechanism for carbonates (**Sec. 2**). Decreasing the particle size of glass and the metal carbonates induces an overall faster surface reaction of the metal carbonate. The formed $CO_2$ inhibits the decomposition of pure $CaCO_3$ [29], but this is not the case for reactive decomposition. Instead, the $CO_2$ is released in an uncontrolled manner, resulting in foam glass with large and open pores.

**Foaming ability**

The ability of a glass melt to foam depends on many parameters. Here, the effects of both isothermal and dynamic heat-treatments on the foaming behaviour are compared among different glasses (Labware, E-glass, CRT panel, soda-lime-silica) prepared with different foaming agents ($MnO_2$, $Na_2CO_3$, $CaCO_3$, dolomit, SiC). The results show (**Table 4.7**) that most glass melt obtain the lowest density (or maximum expansion) in the viscosity

range of $10^{3.7}$-$10^{6}$ Pa s. Scarinci et al [1] claimed that foaming should occur in the range of $10^{3}$-$10^{5}$ Pa s, almost a factor ten lower than in this work. It is unfortunately not reported what those data are based on and a comparison is not possible. Meár reported, that industrial foam glass from Misapor is produced within 1023-1223 K [130] from 98% discarded bottle- and flat glass [130,131] of different colours using SiC/MgO/C as foaming agent [130]. This corresponds to ~$10^{5.9}$ – $10^{3.4}$ Pa s. This agrees fairly well with the results from **Table 4.7**.

In this thesis, heating microscope was used to define a temperature range where optimal foaming should occur. Optimal foaming is defined in this work as a heat-treatment that produces foam glass with closed pores and the lowest possible density. The temperature range was defined from the foaming onset temperature (lower limit) and the maximum expansion rate temperature (upper limit). The maximum expansion rate was linked to a percolation threshold ($\varphi_{cp}$ = 50%). My studies show that the method can be applied to optimise the chemistry of powder mixtures. By analysing the data from Köse [16] the optimal SiC concentration was found to be between 1-4 wt%. This agreed with industrial use [95].

**Thermal conductivity**

The thermal conductivity of foam glass made from CRT panel glass decreases in general linearly within the porosity range of 85-92 % (density range of 0.098-0.45 g/cm$^3$) (**Fig. 5.4**). Different foaming agents ($MnO_2$, $CaCO_3$, $MnO_2$/C and TiN) were used to prepare the foam glasses. The gas composition of foam glass prepared with $CaCO_3$ should mainly contain $CO_2$. The thermal conductivity of these foam glasses did not deviate significantly from foam glasses prepared with $MnO_2$. This was surprising since $O_2$/air atmosphere are more conducting than $CO_2$. The effect of gas composition could be shadowed by the composition alteration of the solid matrix due to incorporation of foaming agent. This means that we should not ignore the effect of foaming agent residues (e.g. $Ca^{2+}$, $Mn^{2+}$/$Mn^{3+}$) on the solid conductivity. More work is necessary to clarify the role of foaming agent.

# 7. Conclusion and Perspectives

We have investigated foam dynamics, foaming ability, thermal conductivity and proposed a reaction mechanism for metal carbonates and metal oxides to clarify the impact of different reaction mechanisms on the foam melt dynamics and resulting properties. The metal carbonates decompose on the particle surface immediately when they are in contact with glass melt. The resulting metal oxide located at the melt-particle surface inhibits further decomposition. However, decomposition continues as fresh melt are in contact with the particle. Fresh melt gets in contact with the particle, when the cations diffuse into the glass melt and when melt flows to the particle. The gas formation at the particle can induce the melt flow. The gas formation of metal oxides is controlled by redox equilibrium and dissolution kinetics. The metal oxides first dissolve into the glass melt and subsequently reduce according to the local reduction potential. In this way, the gas formation is controlled. We show in addition, that nucleation and grow of new bubbles can occur if the metal oxide become incorporated in the melt.

Foaming of CRT panel glass with $MnO_2$ shows that $Mn_2O_3$ dissolves into the glass melt. We show the foam continues to grow even when the majority of the foam percolated. We discuss the impact of $Mn_2O_3$ location on the gas formation. $Mn_2O_3$ becomes incorporated into the glass melt. This enables nucleation and growth of bubbles.

We determined the foaming ability of several glasses for foaming ability in terms of obtaining minimum density. We attempt to find a universal viscosity regime at which foaming of glass melts should proceed. Temperature studies from literature were converted to viscosity and compared with our experimental results. Six out of seven glass melts attained their lowest density in the viscosity regime of $10^{3.7}$-$10^{6}$ Pa s. This result is based on isokom foaming, dynamic heat-treatment and heating microscope results. The foam glass industry uses a diverse range of melt formers and foaming agents. Therefore, these findings are instructive for

optimisation the heating program of industrial foam glass production and assessing the feasibility for implementing new resources in the production line.

Using heating microscope we define several characteristic temperatures of the foaming process. We use these to define a temperature regime for optimal foaming in terms of foam density and closed porosity. These findings provide additional tool for optimising foaming process and will be a useful tool for tuning foaming process and for testing foaming performance of waste materials prior introduction to production line.

We studied the thermal conductivity of foam glasses made from CRT panel glass. It possesses high glass stability (low ability to crystallise) and low thermal conductivity. Based on these properties, CRT panel glass could advantageously be used in the production of foam glass.

The thermal conductivity of foam glass prepared with $CaCO_3$, $MnO_2$ and $MnO_2$/C were compared. The experimental thermal conductivity decreased linearly with foam density. The foaming agents should promote different gas composition in the foam glass. Based on the solid conductance of CRT panel glass, analytical calculations show a ~9 mW/(mK) difference should be observable between foam glass with air/$O_2$ and $CO_2$. However, no difference attributed to gas composition could be observed. We explain this behaviour with the chemical changes to solid matrix caused by the foaming agent. The resulting CaO from $CaCO_3$ decomposition increased the thermal conductivity of the solid matrix, whereas manganese oxide could decrease the thermal conductivity. This effect masks the influence of gas composition on the thermal conductivity of foam glass.

Both the thermal conductivity and the reaction mechanism of $CaCO_3$ and the resulting density and pore structure of the foam glass are disadvantageous for producing insulating foam glass.

# Nomenclature

| | |
|---|---|
| $\eta_g$ | Shear viscosity of bubble- and crystal free glass melt |
| $\eta_\infty$ | Shear viscosity of bubble- and crystal free glass melt |
| $\lambda_f$ | Thermal conductivity of foam |
| $\lambda_g$ | Thermal conductivity of gas |
| $\lambda_s$ | Thermal conductivity of solid |
| $\varphi$ | Porosity of foam |
| $\varphi_{CP}$ | Closed porosity of foam |
| $\rho$ | Density of glass (solid density) |
| $\rho_{foam}$ | Foam density |
| $\rho_{skel}$ | Skeletal density (or pycnometer density) |
| $\rho_{pow}$ | Density of powdered foam glass (solid density) |
| $\tau$ | Tortuosity factor |
| $A$ | Silhouette area obtained with heating microscope |
| $A_0$ | Silhouette area at T=423 K obtained with heating microscope |
| $f_s$ | Denotes the amount of the solid located in the strut |
| $K$ | Fitting parameter |
| $m$ | Fragility index obtained by fitting with Eq. (4.1) |
| $N$ | Number of pores per $mm^2$ |
| $N_A$ | The bubble number density corrected for foam expansion |

| | |
|---|---|
| $t_H$ | Treatment time |
| $T$ | Temperature |
| $T_f$ | Foaming temperature |
| $T_{f,onset}$ | Onset of foaming |
| $T_g$ | Glass transition temperature measured with DSC |
| $T_{g,vis}$ | Glass transition temperature obtained by fitting with Eq. (4.1) |
| $T_{r,max}$ | Temperature of maximum expansion |
| $T_s$ | Onset of sintering |
| $V_0$ | Volume of foam produced at 1063 K for 5 min |
| $V_i$ | Volume of *i*th foam |

# Bibliography

1. G. Scarinci, G. Brusatin, E. Bernardo, Glass Foams, in: M. Scheffler, P. Colombo (Eds.), Cellular Ceramics: Structure, Manufacturing, Properties and Applications, Wiley-VCH Verlag GmbH & Co. KGaA, Weinheim, FRG, 2005, pp. 158-176.

2. A.K. Glüsing, R. Conradt, in: R.K. Dhir, M.C. Limbachiya, T.D. Dyer (Eds.), Recycling and Reuse of Glass Cullet, Thomas Telford, 2001, 29-41.

3. J.R. Mueller, M.W. Boehm, C. Drummond, Waste Manag. 32 (2012) 1560.

4. Herat, S. Recycling of cathode ray tubes (CRTs) in electronic waste. Clean, 2008, 36, 19–24.

5. Industry council for electronic equipment recycling. Materials recovery from waste cathode ray tubes (CRTs). Published by The Waste & Resources Action Programme, 2004, United Kingdom.

6. Xu, Q., Li, G., He, W., Huang, J. & Shi, X. Waste Manag. 2012, 32, 1566–74.

7. F. Méar, P. Yot, M. Cambon, M. Ribes, Wate Manag. 26 (2006) 1468.

8. U. Wiens, Leaching from construction products into soil and ground water, CEN/TC 351/WG 1, NEN, 2013 (Berlin).

9. C. Zhang, J. Wang, J. Bai, J. Guan, W. Wu, C. Guo, Waste Manag. Rec. 31 (2013) 759.

10. M. Chen, F.-S. Zhang, J. Zhu, J. Hazard. Mat. 161 (2009) 1109.

11. H.-Y. Kang, J.M. Schoenung, Resour. Conserv. Recycl. 45 (2005) 368.

12. L. Rocchetti, F. Beolchini Waste Manag. 23 (2014) 468.

13. P.G. Yot, F.O. Méar, J. Hazard. Mat. 185 (2011) 236.

14. E. Bernardo, G. Scarinci, S. Hreglich, Glass Sci. Tech. 78 (2005) 7.

15. J.P. Wu, A.R. Boccaccini, P.D. Lee, R.D. Rawlings, Proc. Eighth Eur. Soc. Glass Sci. Technol. Conf. Glass Technol.: Eur. J. Glass Sci. Technol. A 48 (2007) 133.

16. G. Bayer, S. Köse, Riv. della Staz. Sper. Vetro 5 (1979) 310.

17. S. Köse, Untersuchungen zur Blähdynamik des Schaumglases, (PhD thesis) Eidgenössischen Technischen Hochschule Zürich, 1981. 105-118. [In German]

18. J. König, R.R. Petersen, Y.-Z. Yue, Ceram. Int. 41 (2015) 9793.

19. H. Dennert, H.V. Dennert, A. Seidl, "Method for making shaped foam glass bodies", US patent, 4,430,107, 1982.

20. H. Pieper, "Verfahren und Vorrichtung zum kontinuierlichen Herstellen von Schaumglas", German patent, 2,028,666, 1970.

21. J. König, R.R. Petersen, Y.-Z. Yue, „A method to produce foam glasses", Danish patent, PA 2014 70419, 2014.

22. J. García-Ten, A. Saburit, M.J. Orts, E. Bernardo, P. Colombo, Glass Tech.: Eur. J. Glass Sci. Technol. A 52 (2011) 103.

23. F. Mear, P. Cambon, B. Liautard, Verre, 9 (2003) 72. [In French]

24. J. König, R.R. Petersen, Y. Yue, J. Eur. Ceram. Soc. 34 (2014) 1591.

25. S. Köse, G. Bayer, Glastchn. Ber. 7 (1982) 151. [In German]

26. M. Tasserie, D. Bideau, J. Rocherullé, P. Verdier, Y. Laurent, Verre, 6 (1992) 9. [In French]

27. A.A. Ketov, in: R.K. Dhir, M.C. Limbachiya, T.D. Dyer (Eds.), Recycling and Reuse of Glass Cullet, Thomas Telford, 2001, 85-91.

28. J.-W. Kim, Y.-D.D. Lee, H.-G. Lee, ISIJ Int. 41 (2001) 116.

29. B.V. L'vov, Thermal Decomposition of Solids and Melts – New Thermochemical Approach to the Mechanism, Kinetics and Methodology, Springer, 2007.

30. T. Shirai, S. Tachibana, A. Tsuchiyama, Evaporation Rates of Na From $Na_2O$-$SiO_2$ Melt at 1 Atm, 31st Annual Lunar and Planetary Science Conference, Houston, Texas, March 13-17, 2000.

31. O.S. Verheijen "Thermal and Chemical behavior of glass forming batches", PhD thesis, Technische Univirsiteit Eindhoven (2003), pp. 42-48.

32. R. Conradt, in: Fundamentals of Glass Science and Technology, Proceedings of the 4th Conference of European Society of Glass Technology (ESG), Glafo, Växjö, Sweden, 1997, p. 290.

33. S. Gelnar, E. Smrckova, Glass Int. 33 (2010) 15.

34. M.D. Dolan, S.T. Misture, Glass Tech. 45 (2004) 212.

35. M.D. Dolan, S.T. Misture, Glass Tech. 45 (2004) 167.

36. E. Bernardo, F. Albertini, Ceram. Int. 32 (2006) 603.

37. E. Bernardo, G. Scarinci, S. Hreglich, Glass Tech. 78 (2005) 7.

38. M. Chen, F.-S. Zhang, J. Zhu, in: L. Zhang, G.K. Krumdick (Eds.), Reycling of Electronic Waste II, Proceedings of the Second Symposium, The Minerals, Metals & Materials Scoiety, 2011, 97-102.

39. C. Mugoni, M. Montorsi, C. Siligardi, F. Andreola, I. Lancellotti, E. Bernardo, L. Barbieri, 41 (2015) 3400.

40. H.R. Fernandes, D.D. Ferreira, F. Andreola, I. Lanceelotti, L. Barbieri, J.M.F. Ferreia, Ceram. Int. 40 (2014) 13371.

41. H.R. Fernandes, F. Andreola, L. Barbieri, I. Lancellotti, M.J. Pascual, J.M.F. Ferreira, Ceram. Int. 39 (2013) 9071.

42. A. Ayadi, N. Stiti, K. Boumchedda, H. Rennai, Y. Lerari, Pow. Tech. 208 (2011) 423.

43. N.M.P. Low, J. Mat. Sci. 16 (1981) 800.

44. C.-T. Lee, J. Ind. Eng. Chem. 19 (2013) 1916.

45. H.R. Fernandes, D.U. Tulyaganov, J.M.F. Ferreira, Ceram. Int., 35 (2009) 229.

46. A. Pokorny, J. Vicenzi, C.P. Bergmann, Waste Manag. & Res. 29 (2011) 172.

47. Y.A. Spiridonov, L.A. Orlova, Glass Ceram. 60 (2003) 313.

48. E. Bernardo, R. Cedro, M. Florean, S. Hreglich, Ceram. Int., 33 (2007) 963.

49. A.S. Llaudis, M.J.O. Tari, F.J.G. Ten, E. Bernardo, P. Colombo, Ceram. Int. 35 (2009) 1953.

50. E. Bernardo, G. Scarinci, P. Bertuzzi, P. Ercole, L. Ramon, J. Porous Mater. 17 (2010) 359.

51. E.R. Stobbe, B.A. de Boer, J.W. Geus, Catal. Today 47 (1999) 161.

52. F. Tedjar, J. Guitton, Thermchim. Acta. 181 (1991) 13.

53. W.D. Johnston, J. Am. Ceram. Soc. 48 (1965), 184.

54. R.K. Chinnam, S. Molinaro, E. Bernardo, A.R. Boccaccini, Ceram. Trans. 246 (2014) 205.

55. M. Marangoni, M. Secco, M. Parisatto, G. Artioli, E. Bernardo, P. Colombo, H. Altlasi, M. Binmajed, M. Binhussain, J. Non-Cryst. Solids 403 (2014) 83.

56. R.D. Shannon, Acta Cryst. 32 (1976) 751.

57. J. Kappel, R. Conradt, H. Scholze, Gastech. Ber. 60 (1987) 189.

58. P.R. Laimböck, Foaming of Glass Melts, (PhD thesis) Technische Universiteit Eindhoven, 1998. 180-181.

59. F. Pigeonneau, H. Kočárková, F. Rouyer, Colloid. Surface. A: Physicochem. Eng. Aspects 408 (2012) 8.

60. J.S. Schaaf, R.G.C. Beerkens, J. Col. Int. Sci. 295 (2006) 218.

61. H. Kočárková, F. Rouyer, F. Pigeonneau, Phys. Fluids, 25 (2013) 022105.

62. H. Kočárková, Stability of glass foams: Experiments at the bubble scale and on vertical film, (PhD thesis) Université Paris-Est, 2011.

63. J.P. Wu, A.R. Boccaccini, P.D. Lee, M.J. Kershaw, R.D. Rawlings, Adv. Apl. Ceram. 105 (2006) 32.

64. M. Tasserie, D. Bideau, Y. Laurent, P. Verdier, High Temp. Chem. Processes, 1 (1992) 241.

65. J.M. Castro, A. Burgisser, C.I. Schipper, S. Mancini, Bull. Volcanol. 74 (2012) 2339.

66. R.J. Pugh, Adv. Colloid Interfac. 64 (1996) 67.

67. A.A. Proussevitch, D.L. Sahagian, V.A. Kutolin, J. Volcanol. Geoth. Res. 59 (1993) 161.

68. J. Deubener, R. Brückner, H. Hessenkemper, Glastech. Ber. 65 (1992) 9.

69. Y. Imanaka, S. Aoki, N. Kamehara, K. Niwa, J. Am. Ceram. Soc. 78 (1995) 1265.

70. J.F. Larsen, M.-H. Denis, J.E. Gardner, Geochim. Cosmochim. Ac. 68 (2004) 333.

71. J.C. Mauro, Y.Z. Yue, A.J. Ellison, P.K. Gupta, D.C. Allan, Proc. Natl. Acad. Sci. U.S.A. 106 (2009) 19780.

72. Q. Zheng, J.C. Mauro, A.J. Ellison, M. Potuzak, Y.Z. Yue, Phys. Rev. B, 83 (2011) 212202.

73. D.C. Allan, J. Non-Cryst. Solids, 358 (2012) 440.

74. Y. Imanaka, K. Yamazaki, S. Aoki, N. Kamehara, K. Niwa, Nippon Seram. Kyo. Gak. 97 (1989) 309.

75. J.-H. Jean, T.K. Gupta, J. Am. Ceram. Soc. 76 (1993) 2010.

76. M.I. Martín, F.A. López, F.J. Alguacil, M. Romero, Ceram. Int. 40 (2014) 2769.

77. R. Müller, R. Meszaros, B. Peplinski, S. Reinsch, M. Eberstein, W. Schiller, J. Deubener, J. Am. Ceram. Soc. 92 (2009) 1703.

78. E.D. Zanotto, J. Non-Cryst. Solids, 129 (1991) 183.

79. M.O. Prado, C. Fredericci, E.D. Zanotto, J. Non-Cryst. Solids, 331 (2003) 145.

80. A. Kucuk, A.G. Clare, L. Jones, Glass Tech. 40 (1999) 149.

81. N.M. Parikh, J. Am. Ceram. Soc. (1958) 18.

82. J. Kraxner, M. Liska, R. Klement, M. Chromciková, Ceramics – Silikáty, 53 (2009) 141.

83. A. Dietzel, Sprechsaal, 75 (1942) 82. [In German]

84. K.C. Lyon, J. Am. Ceram. Soc. 27 (1944) 186.

85. V.I. Goleus, A.Y. Belyi, É.M. Sardak, Y.I. Belyi, Glass Ceram. 53 (1996) 226.

86. C.F. Cooper, J.A. Kitchener, J. Iron Steel Inst. 193 (1959) 48.

87. S.-H. Yi, S.-M. Kim, Scand. J. Metall, 31 (2002) 148.

88. J. Frenkel, J. Phys. (Moscow), 9 (1945) 385.

89. J.K. Mackenzie, R. Shuttleworth, Proc. Phys. Soc. B 62 (1949) 833.

90. M.O. Prado, E.D. Zanotto, C.R. Chimie 5 (2002) 773.

91. R. Müller, M. Eberstein, S. Reinsch, W.A. Schiller, J. Deubener, A. Thiel, Phys. Chem. Glasses: Eur. J. Glass Sci. Technol. B 48 (2007) 259.

92. M.O. Prado, M.L.F. Nascimento, E.D. Zanotto, J. Non-Cryst. Solids, 354 (2008) 4589.

93. A. Fluegel, Proc. Eighth Advances in Fusion and Processing of Glass, Glass Technol.:Eur. J. Glass Sci. Technol. A, 48 (2007) 13.

94. Y. Attila, M. Güden, A. Tasdemirci, Ceram. Int. 39 (2013) 5869.

95. News article about TECHNOpor (www.technopor.com) - http://www.openpr.de/news/508390/TECHNOpor-erhaelt-EPD-Umwelt-Produktdeklaration-Glasschaum-Granulat-von-TECHNOpor-ist-durchweg-umweltfreundlich.html

96. H. Hojaji, Mater. Res. Soc. Symp. Proc., 136 (1988) 185.

97. F. Mear, P. Yot, R. Viennois, M. Ribes, Ceram. Int. 33 (2007) 543.

98. C. Vancea, I. Lazău, Cent. Eur. J. Chem, 12 (2014) 804.

99. J.C. Mauro, E.D. Zanotto, Int. J. Appl. Glass Sci. 5 (2014) 313.

100. M.K. Choudhary, R.M. Potter, Heat Transfer in Glass-Forming Melts, in: L.D. Pye, A. Montenero, I. Joseph (Eds.), Properties of Glass-Forming Melts, CRC Press, Taylor & Francis, 2005, chapter 9.3.1.

101. K.-I. Horai, J. Geophys. Res. 76 (1971) 1278.

102. D.G. Cahill, Mat. Res. Soc. Bul. 37 (2012) 855.

103. A.K. Varshneya, Fundamental of Inorganic Glasses, Academic Press, London, 1994.

104. D.P.H. Hasselman, K.Y. Donaldson, J.R. Thomas, J.J. Brennan, J. Am. Ceram. Soc. 79 (1996) 742.

105. D.P.H. Hasselman, L.F. Johnson, J. Compos. Mater. 21 (1987) 508.

106. D.S. Smith, A. Alzina, J. Bourret, B. Nait-Ali, F. Pennec, N. Tessier-Doyen, K. Otsu, H. Matsubara, P. Elser, U.T. Gonzenbach, J. Mater. Res. 28 (2013) 2260.

107. R.G. Griskey, Transport Phenomena and Unit operations: A Combined Approach, John Wiley & Sons, Inc. 2002, Chp. 9.

108. P.G. Collishaw, J.R.G. Evans, J. Mat. Sci. 29 (1994) 2261.

109. E. Placido, M.C. Arduini-Schuster, J. Kuhn, Infrared Phys. Techn. 46 (2005) 219.

110. M. Bouquerel, T. Duforestel, D. Baillis, G. Rusaouen, Energ. Buildings 54 (2012) 320.

111. R.W. Skochdopole, Chem. Eng. Prog. 57 (1961) 55.

112. B. Nait-Ali, K. Haberko, H. Vesteghem, J. Absi, D.S. Smith, J. Eur. Ceram. Soc. 26 (2006) 3567.

113. J. Fricke, U. Heinemann, H.P. Ebert, Vacuum 82 (2008) 680.

114. H.W. Russell, J. Am. Ceram. Soc. 18 (1935) 1.

115. R. Landauer, J. Appl. Phys. 23 (1952) 779.

116. M.A. Schuetz, L.R. Glicksman, J. Cell. Plast. 20 (1984) 114.

117. M.A. Schuetz, Heat transfer in Foam Insulation, (Master Thesis) Massachusetts Institute of Technology, 1979.

118. E. Solórzano, M.A. Rodriguez-Perz, J. Lázaro, J.A. de Saja. Adv. Eng. Mat. 11 (2009) 818.

119. Y. Hiroshima, Y. Hamamoto, S. Yoshida, J. Matsuoka, J. Non-Cryst. Solids 354 (2008) 341.

120. V.I. Primenko, Glass Ceram. 37 (1980) 240.

121. M. Alvarez-Lainez, M.A. Rodriguez-Perez, J.A. de Saja, J. Pol. Sci.: Part B: Pol. Phys, 46 (2008) 212.

122. J. Kuhn, H.-P. Ebert, M.C. Arduini-Schuster, D. Büttner, J. Fricke, Int. J. Heat Mass Transfer 35 (1992) 1795.

123. J. König, R.R. Petersen, Y.Z. Yue, Lightweight foam glasses with low thermal conductivity, (2015) *under preparation*.

124. A.F. Holleman, E. Wiberg, Lehrbruch der Chemie, Teil 1: Anorganische Chemie, Walter de Gruyter & Co, 1952, p 297-298.

125. N.A. Ghoneim, A.A. Ahmed, S. Gharib, Thermochim. Acta 71 (1983) 43.

126. E.H. Ratcliffe, Glass Tech. 4 (1963) 113.

127. M.M. Ammar, S.A. Gharib, M.M. Halawa, H.A. El-Batal, K. El-Badry, J. Am. Ceram. Soc. (1983) C-76.

128. S.M. Salman, S. Gharib, Thermochim. Acta 77 (1984) 227.

129. P.F. van Velden, Glass Tech. 6 (1965) 166.

130. F. Mear, Etude de mousses de verres issus de Tubes à Rayons Cathodiques (TRC) en fin de vie contenant de l'oxyde de plomb: Elaboration, caractérisations physicochimiques et applications, (PhD thesis), Université de Montpellier II, 2004. [In French]

131. www.Misapor.com [assessed June 10,2015]

# List of Publications

## Publications in Peer-review journals

1) J. König, R.R. Petersen, Y.Z. Yue, Lightweight foam glasses with low thermal conductivity, (2015) *under preparation*.

2) J. König, R.R. Petersen, Y.Z. Yue, Fabrication of highly insulating foam glass made from CRT panel glass, Ceram. Int. 41 (2015) 9793.

3) J. König, R.R. Petersen, Y.Z. Yue, Influence of the glass–calcium carbonate mixture's characteristics on the foaming process and the properties of the foam glass, J. Eur. Ceram. Soc, 34 (2014) 1591.

## Patent

4) J. König, R.R. Petersen, Y.Z. Yue, „A METHOD TO PRODUCE FOAM GLASSES", PA 2014 70419 (Danish patent).

## Oral and poster presentations at conferences:

5) R.R. Petersen, J. König, Y.Z. Yue, Nordic Conference on Ceramic and Glass Technology, **Oral presentation**, "Optimized Synthesis of Foam Glass from Recycled CRT Panel Glass ", Risø, 6-7th December, 2012

6) R.R. Petersen, J. König, M.M. Smedskjaer, Y.Z. Yue, 87. Glastechnischen Tagung, **Poster**, "Insights into reaction mechanism of $Na_2CO_3$ in foaming process of cullet powder", Bremen, 29-31st May, 2013

7) R.R. Petersen, J. König, M.M. Smedskjaer, Y.Z. Yue, 23rd international Conference on Glass, **Poster**, "Foaming of CRT panel glass powder with $Na_2CO_3$", Prague, 1-5th July, 2013

8) R.R. Petersen, J. König, M.M. Smedskjaer, Y.Z. Yue, DGG–ACerS GOMD meeting, **Oral Presentation**, "Viscous Control of the Foam Glass Process ", Aachen, 25-30 May 2014

9) R.R. Petersen, J. König, M.M. Smedskjaer, Y.Z. Yue, DGG–ACerS GOMD meeting, **Poster**, "Thermal conductivity of Foam Glass", Aachen, 25-30 May 2014

10) R.R. Petersen, J. König, Y.Z. Yue, Danish Ceramic Society, Annual Meeting, **Oral presentation**, "Recycle Glass in Foam Glass Production", DTU Risø, 12 June 2014